

Catalog of Equation Based Lattice Structures and Their Homogenized Properties Sorted by Parent TPMS

Joseph W. Fisher^{*12}, Simon W. Miller², Joseph Bartolai², Timothy W. Simpson¹³, Michael A. Yukish²

Contents

1 Introduction	1
2 Catalog of Lattice Structures and Property Data	3
2.1 Gyroid	5
2.2 D	7
2.3 P	8
2.4 IWP	9
2.5 Neovius	11
2.6 C(Y)	12
2.7 Lidinoid	14
2.8 OCTO	16
2.9 FRD	19
2.10 S	21
2.11 P+C(P)	22
2.12 Split-P	24
2.13 F	25
2.14 C(D)	27
2.15 G'	29
2.16 G'_2	30
2.17 D'	31
2.18 K	32
2.19 C(S)	33
2.20 Y	35
2.21 ±Y	37
2.22 C(±Y)	38
2.23 C(I ₂ -Y**)	39
2.24 W	41
2.25 Q*	42
2.26 C(G)	43
2.27 Slotted-P	45
2.28 Double Versions of the Gyroid, D, and P	46
2.29 Modifications to Surface Equations at Low Volume Fractions	47
3 Images of Lattice Structures and Related TPMS	48
Bibliography	55

* Corresponding author: jwf23@psu.edu

¹ Department of Mechanical Engineering, The Pennsylvania State University, University Park, PA 16802, USA

² Applied Research Laboratory, The Pennsylvania State University, State College, PA 16803, USA

³ Department of Industrial and Manufacturing Engineering, The Pennsylvania State University, University Park, PA 16802, USA

1 Introduction

The design of lattice structures for additive manufacturing has grown into an active field of research. One particular group of lattice structures that have shown promise are those based on Triply Periodic Minimal Surfaces (TPMS) that exhibit two attractive characteristics. First, a surface that is triply periodic has a pattern that repeats throughout a 3D real space (\mathbb{R}^3), allowing the surface to fill whatever domain is of interest. Second, a minimal surface has zero mean curvature at all points, meaning it does not have sharp edges that would act as stress risers. Compared to similar topologies based on uniform beams, lattices based on TPMS have shown more uniform stress distributions (Guo et al., 2019) and can be used to divide space into multiple closed volumes making them of particular interest in heat exchanger applications (Dutkowski et al., 2022, Yeranee and Rao, 2022). While a TPMS can be modeled in \mathbb{R}^3 , because it is only a surface, it has no thickness. As a result, it is non-physical and cannot actually exist in the physical world. However, we can apply two level sets denoted as t_1 or t_2 where each defines an isosurface of the TPMS, and then define the region between these two surfaces to be solid, producing a “child” structure from the “parent” TPMS. Closed-form representations are only known for a few TPMS and they are difficult to work with directly (von Schnering and Nesper, 1991). To enable modeling of TPMS-like structures, approximations to TPMS have been derived that are implicitly defined (von Schnering and Nesper, 1991, Wohlgemuth et al., 2001). Level sets are easily applied to these approximations by adding or subtracting a level set value from the equation. The choice of the two level sets defines both the type of structure and the volume of the domain that is solid vs the total volume of the domain – the ratio of which is denoted as the Volume Fraction (VF) and is a key parameter used in the design of lattice structures. This solid region defined by two level sets can be expressed as an equation with two inequalities applied to the implicit equation $f(x, y, z)$ approximating the TPMS (Eq. 1).

$$t_1 \leq f(x, y, z) \leq t_2 \quad (1)$$

TPMS structures are periodic and can be represented by a single period (in each dimension) that fully captures the geometry of the larger structure. To capture all of the unique geometry of the lattice, we define a volume that is one period in each of the coordinate directions of the coordinate system, and we call this volume the unit cell (others may refer to this as a representative volume element). The unit cell provides a convenient tool for visualizing and discussing lattice structures. Here we use the Cartesian coordinate system and cubic unit cells where the periods in x , y , and z are equal. These equations can be transformed into cylindrical or spherical coordinates, and the periods need not be equal. Changes to the proportionality of the periods in different directions in Cartesian coordinates have been shown to have a significant impact on the mechanical response of a lattice (Chen et al., 2022) as well as the flow of fluids through the lattice (Mahmoud et al., 2023).

There are three special cases of Eq. 1, classified based on the level set values applied, that we discuss in the dataset and this document, and these three cases are:

- Triply Periodic endo-Skeleton (TPnS)

$$t_{\text{endo}_{\text{crit}}} \leq f(x, y, z) \leq t \quad (2)$$

- Triply Periodic Surface (TPSf)

$$-|t| \leq f(x, y, z) \leq |t| \quad (3)$$

- Triply Periodic exo-Skeleton (TPxS)

$$t \leq f(x, y, z) \leq t_{\text{exo}_{\text{crit}}} \quad (4)$$

where $t_{\text{endo}_{\text{crit}}} < t < t_{\text{exo}_{\text{crit}}}$. Because of the 3D periodicity of these surfaces, there are two critical level set values beyond which changes to the magnitude of the level set will have no effect on the geometry. The values of the two critical level sets are dependent on the equation of interest and are given in Section 2.

These three classifications provide a framework for the definition, discussion, and implementation of surface based lattice structures. Different naming conventions have been used previously in the literature

and we note them in [Table 1](#). This new naming scheme that we propose fits with how lattices are utilized in literature and application with two major benefits: the differentiation between the two different skeletal lattices and the use of “endo” and “exo” mirror the sign convention of the implicit equations.

Table 1: Alternative naming conventions that have been used to identify the surface and skeletal lattices derived from the TPMS. In addition to using the TPMS name for any of the three lattices, most conventions do not differentiate between the TPnS and TPxS.

TPSF	TPnS or TPxS
matrix	network
matrix phase	network phase
double	single
sheet	strut
walled	offset
shell	solid
	net
	tubular & inverse tubular

Each of the lattice types in Eqs. 2 thru 4 has a single independent variable t . However, the case where the two level sets in [Eq. 1](#) are unequal and between the critical limits has two independent variables and is not captured in Eqs. 2 thru 4. The generation of lattices that do not fall into these categories is uncommon in literature, and the control of two independent level sets makes direct application of [Eq. 1](#) unwieldy. To simplify this, we can reformulate [Eq. 1](#) as two equal and opposite level sets that are centered on some level set value ϵ offset from the $t = 0$ level surface, as shown in [Eq. 5](#).

$$-|t| \leq f(x, y, z) - \epsilon \leq |t| \quad (5)$$

We denote lattices that are generated by [Eqs. 1](#) and 5 that do not fall into the classifications of Eqs. 2 thru 4 as Triply Periodic Eccentric Surfaces (TPcS). Because these TPcS have two independent variables defining the geometry, it is harder to characterize and utilize, and little research has been presented in which the level sets for a surface lattice are not kept symmetric about zero ([Liu et al., 2022](#), [Peng et al., 2019](#)). As a result, we present only information pertaining to the symmetric version of the surface and motivate further study of the impacts of asymmetric level sets.

In this document, we compile the information contained in the dataset provided alongside *Catalog of Triply Periodic Minimal Surfaces, Equation-Based Lattice Structures, and Their Homogenized Property Data*¹ into a format that is easier to interpret. The dataset is stored on GitHub² and includes the plots and images in full resolution and the data presented here in various file formats, along with 3D mesh files for visualization and CAD files for generating these lattices. In [Section 2](#) we report data on lattice structures, and [Section 3](#) contains images of lattices and TPMS. The data in [Section 2](#) are grouped into subsections dedicated to lattices derived from one of the Triply Periodic Minimal Surfaces (TPMS) or unique implicit equations that have been identified in the literature. The images of lattices in [Section 3](#) are sorted to match the order in [Section 2](#). This catalog of surfaces does not cover all TPMS that have been discovered, rather it is focused on TPMS for which an approximate equation exists. Images and descriptions of additional TPMS not included here can be found on Ken Brakke’s website ([Brakke, a](#)).

¹ <https://doi.org/10.1016/j.dib.2023.109311>

² <https://github.com/jwf23/Equation-Based-Lattice-Structure-Dataset>

2 Catalog of Lattice Structures and Property Data

The following subsections of this document are each dedicated to a brief discussion of the lattice structures generated from one of the 27 Triply Periodic Minimal Surface (TPMS) or unique implicit equations that have been identified in the existing literature. Each subsection starts on a new page and includes a summary table containing:

- Different names used in literature to reference the TPMS or its lattices
- The recommended equation for modeling lattices
- Plots of volume fraction vs. level set
- Plots of normalized elastic properties vs. volume fraction
- Critical level set values
- Pinch level set values and associated skeletal volume fractions

In the remaining two subsections [Sections 2.28](#) and [2.29](#) we discuss the double versions of the Gyroid, D, and P surfaces and different methods that have been applied to modify the equations presented here.

The summary tables contain two or three columns if the TPMS is congruent or non-congruent, respectively. A congruent TPMS means the two volumes on the positive and negative sides of the surface have the same shape and size, and one can be transformed into the other without deforming it by some combination of translation, rotation, and reflection. As a direct consequence, the TPnS and TPxS are congruent and therefore share a column for these surfaces.

This catalog of surfaces does not cover all TPMS that have been discovered. It is focused instead on TPMS for which an approximate equation exists and in most cases has been shown in the literature to be of interest. Images and descriptions of additional TPMS not included here can be found on Ken Brakke's website ([Brakke, a](#)). Some equations compiled herein were derived by the combination of other approximate equations ([Wohlgemuth et al., 2001](#)). Two such surfaces are the P+C(P) and Split-P surfaces, for which the existence of a related minimal surface has not been shown. We include these equations on the basis that they are triply periodic and possess finite curvature within \mathbb{R}^3 , similar to equations derived by approximating known TPMS.

In this work, we adopt shorthand notations for the trigonometric functions as follows:

$$S_{ni} = \sin\left(\frac{2\pi n}{d_i} i\right) \quad (6)$$

$$C_{ni} = \cos\left(\frac{2\pi n}{d_i} i\right) \quad (7)$$

where i is a spatial coordinate (i.e. x, y, z), d_i is the size of the lattice's unit cell in direction i , and n is the number of periods of the trigonometric function in the distance d_i (e.g. 1, 2), when n is one, it is omitted from the following equations for simplicity.

Most of the equations listed in this catalog have two pinch points off: one endo and one exo. However, there are eight surfaces that have additional pinch points. Four of the eight become two structures, after reaching their exo pinch point, that independently remain connected until a second exo pinch point. The four surfaces are the Lidinoid, Split-P, G', and G'_2. The other four surfaces, the C(Y), C(D), D', and C(G), have two endo and two exo pinch points. For values between either respective pair of pinch points, these surfaces result in two connected structures as well as disconnected floating masses. The additional pinch points are noted in their respective summary tables, and we discuss the pinch behavior of the two groups in [Section 2.7](#) and [Section 2.6](#) respectively.

Changes to the topology of the lattice that does not result in a change to the number of solid bodies do occur prior to pinch-off for some lattices, like the Lidinoid. Holes form in the “nodes” of the Lidinoid TPxS at a level set of $t = 1.8$. This type of topology change is not captured in the dataset presented here.

While we report specific values for the pinch and critical points, it is important to note that most workflows for additive manufacturing will require discretizing the lattice (typically by meshing the surface of

the lattice with triangles) and, depending on the method of discretization and the resolution, the level sets at which the pinch and critical transitions occur can change. This results in a significant deviation from the intended geometry and performance.

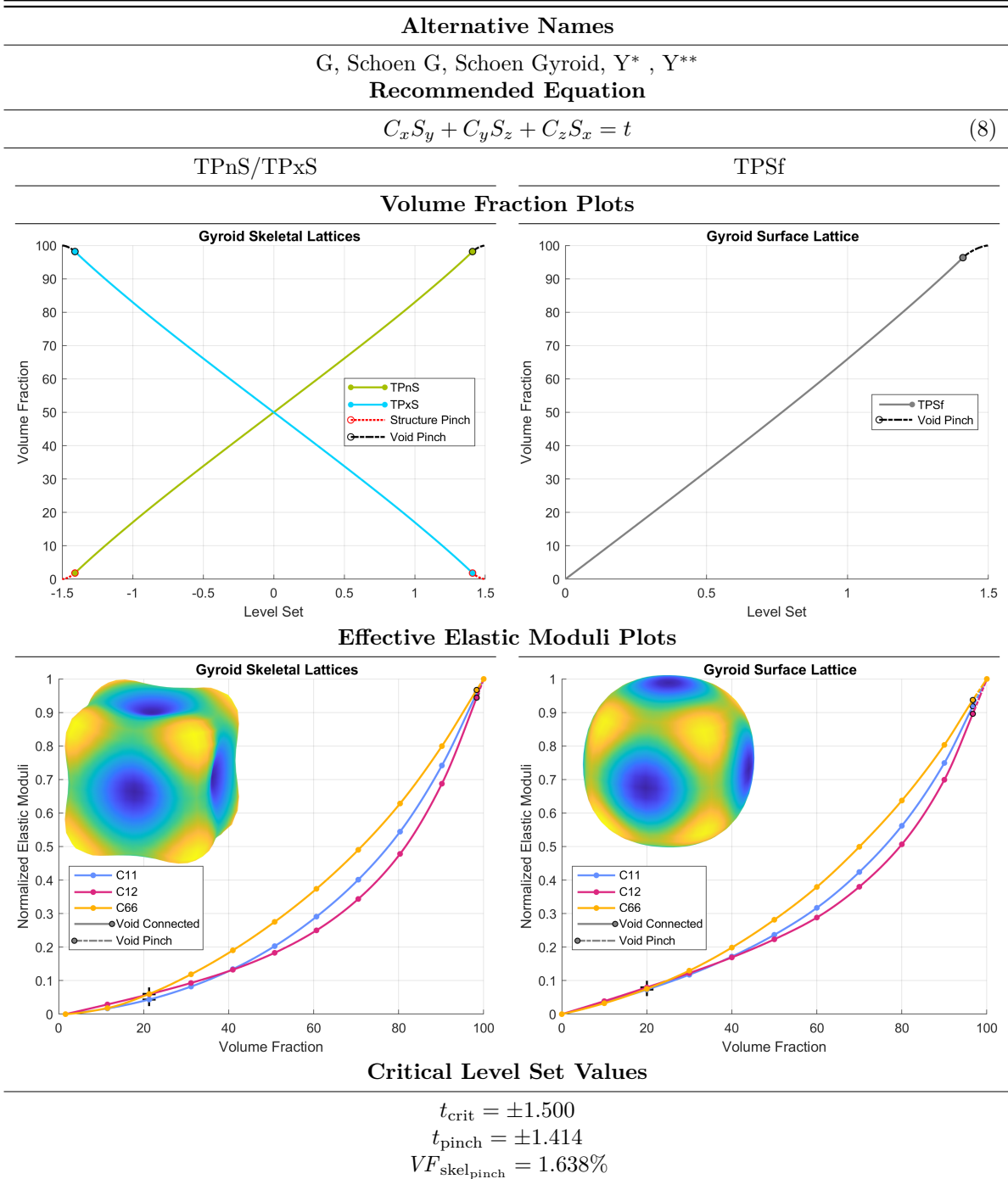
The volume fraction and effective modulus plots presented in each summary table have a couple of unique features to which we call the reader's attention. The curves of the volume fraction vs. level set plots are broken into three sections, one in the color matching the lattice type shown in [Section 3](#), and sections where either the structure or the void space pinches off (becomes discontinuous) which is noted by a change of color and line type. The effective moduli plots shown in the summary tables are generated using the normalized C_{11} , C_{12} , and C_{66} , values from the homogenized constitutive matrices in the dataset. In the homogenization, a Poisson's ratio of 0.35 was used. In these plots, the curves are solid where the void regions are connected, and dash-dotted when the voids become discontinuous. The smooth curves on the effective modulus plots were generated using a shape-preserving piece-wise cubic interpolation³. Overlaid on each plot is a 3D visualization of the anisotropy of the lattice's Young's Modulus. The overplotted anisotropy surface gives only a snapshot at a single volume fraction. We elected to use a volume fraction that is 20% of the way from the smallest volume fraction where the lattice is connected (where the structure pinches off), to fully dense (where the Volume Fraction is 100%). This is marked on the three curves for each lattice with black plus signs. The anisotropy surfaces are oriented to match the images of the surface and lattices in [Section 3](#).

Remainder of page intentionally left blank

³ Using the `pchip` method implemented in MATLAB's `interp1` function

2.1 Gyroid

Table 2: Summary for the Gyroid



Li et al. (2018) developed an equation for the skeletal lattices which features a penalty function, preventing the Gyroid from pinching off at $|t| \geq 1.41$, reproduced in Eq. 9 and allowing for lower density skeletal lattices. They also produced a fit for the relationship between the level set and volume fraction of the skeletal Gyroid (Eq. 10).

$$F = \begin{cases} \text{Eq. 8} & |t| < 1.41 \\ C_x S_y + C_y S_z + C_z S_x - \\ (0.45t - 0.58) (C_{2x} C_{2y} + C_{2y} C_{2z} + C_{2z} C_{2x}) = t & |t| \geq 1.41 \end{cases} \quad (9)$$

$$VF = 0.3325t + 0.5001 \quad (10)$$

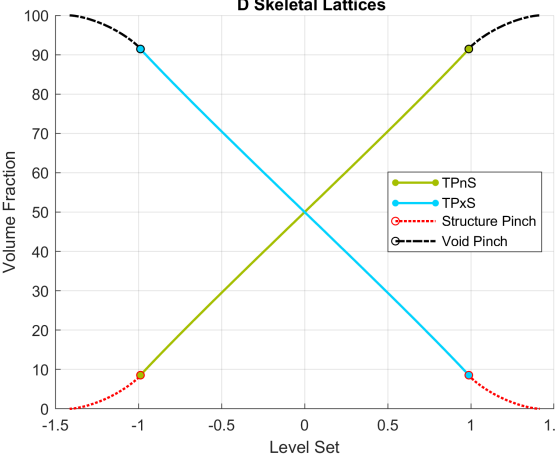
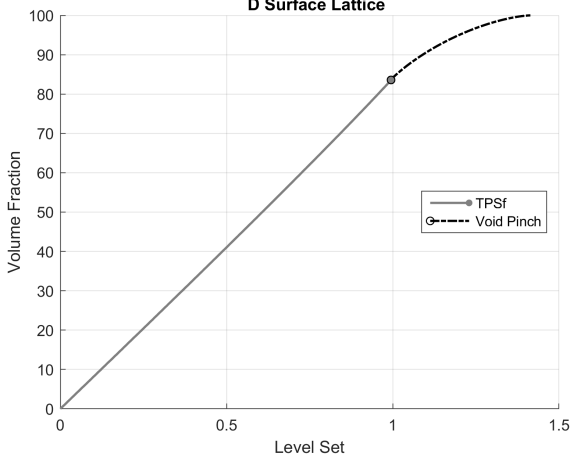
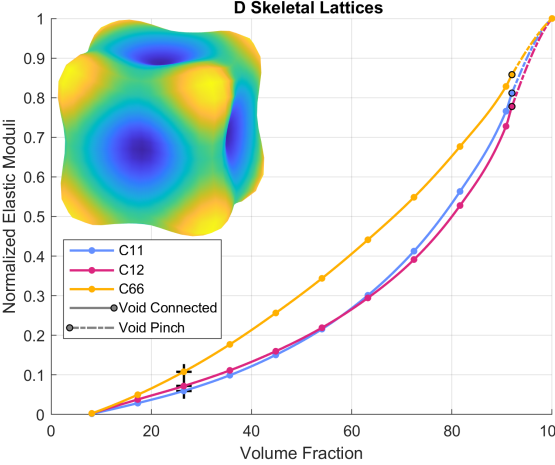
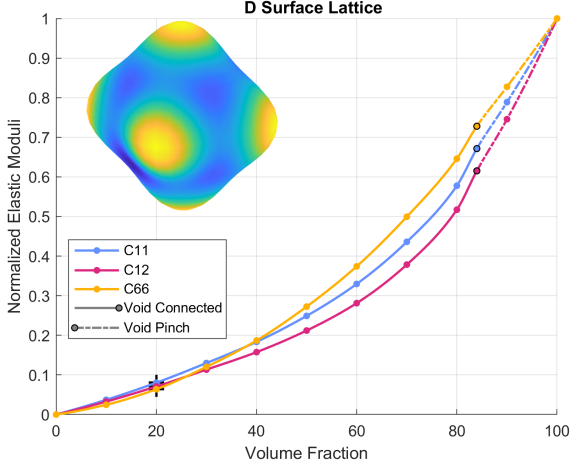
Liu et al. (2022) studied the effect of offsetting the gyroid producing TPcS lattices – they refer to these as “sheet lattices”. In their study, they use a variation of Eq. 9 where the second term is multiplied by a constant (see Eq. 11). Unlike Eq. 9, the second term is present *at all level set values* resulting in changes to the lattice geometry for all volume fractions. The original source of Eq. 11 is, however, not provided in Liu et al. (2022).

$$C_x S_y + C_y S_z + C_z S_x + 0.08 (C_{2x} C_{2y} + C_{2y} C_{2z} + C_{2z} C_{2x}) \quad (11)$$

Remainder of page intentionally left blank

2.2 D

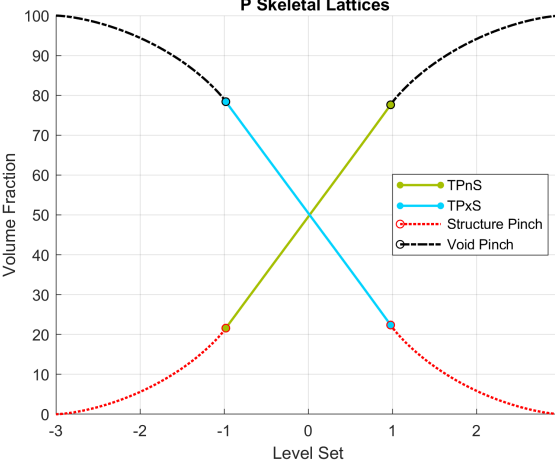
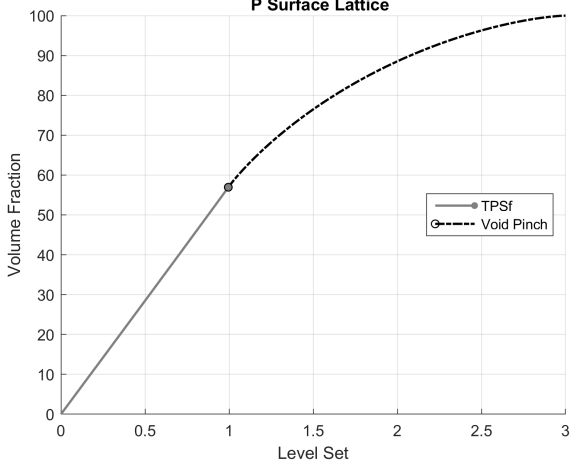
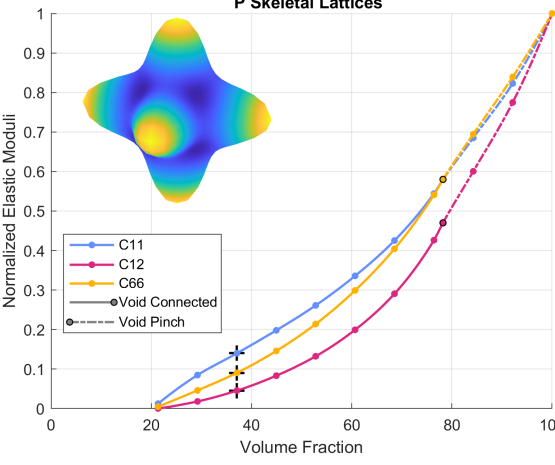
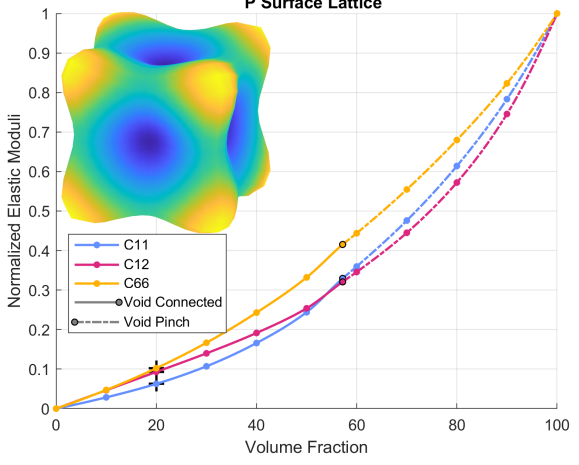
Table 3: Summary for the D Surface

Alternative Names	
Schwarz D, Schwarz Diamond, Diamond, D*	
Recommended Equation	
$S_x S_y S_z + S_x C_y C_z + C_x S_y C_z + C_x C_y S_z = t$	(12)
TPnS/TPxS	TPSf
Volume Fraction Plots	
	
Effective Elastic Moduli Plots	
	
Critical Level Set Values	
$t_{\text{crit}} = \pm 1.414$ $t_{\text{pinch}} = \pm 0.999$ $VF_{\text{skel,pinch}} = 8.101\%$	

We have elected to refer to this as the D–surface rather than the diamond surface to differentiate the lattices generated from it from the strut-based diamond lattice found in the literature (e.g. Liu et al. (2018)).

2.3 P

Table 4: Summary for the P Surface

Alternative Names	
Primitive, Schwarz, Schwarz P, Simple Cubic, P*	
Recommended Equation	
$C_x + C_y + C_z = t$	(13)
TPnS/TPxS	TPSf
Volume Fraction Plots	
	
Effective Elastic Moduli Plots	
	
Critical Level Set Values	
$t_{\text{crit}} = \pm 3.000$ $t_{\text{pinch}} = \pm 1.000$ $VF_{\text{skel,pinch}} = 21.36\%$	

We have elected to refer to this as the P–surface rather than the primitive surface to differentiate the lattices generated from it from the strut-based primitive lattice found in the literature (e.g. [Austermann et al. \(2019\)](#)).

2.4 IWP

Table 5: Summary for the IWP

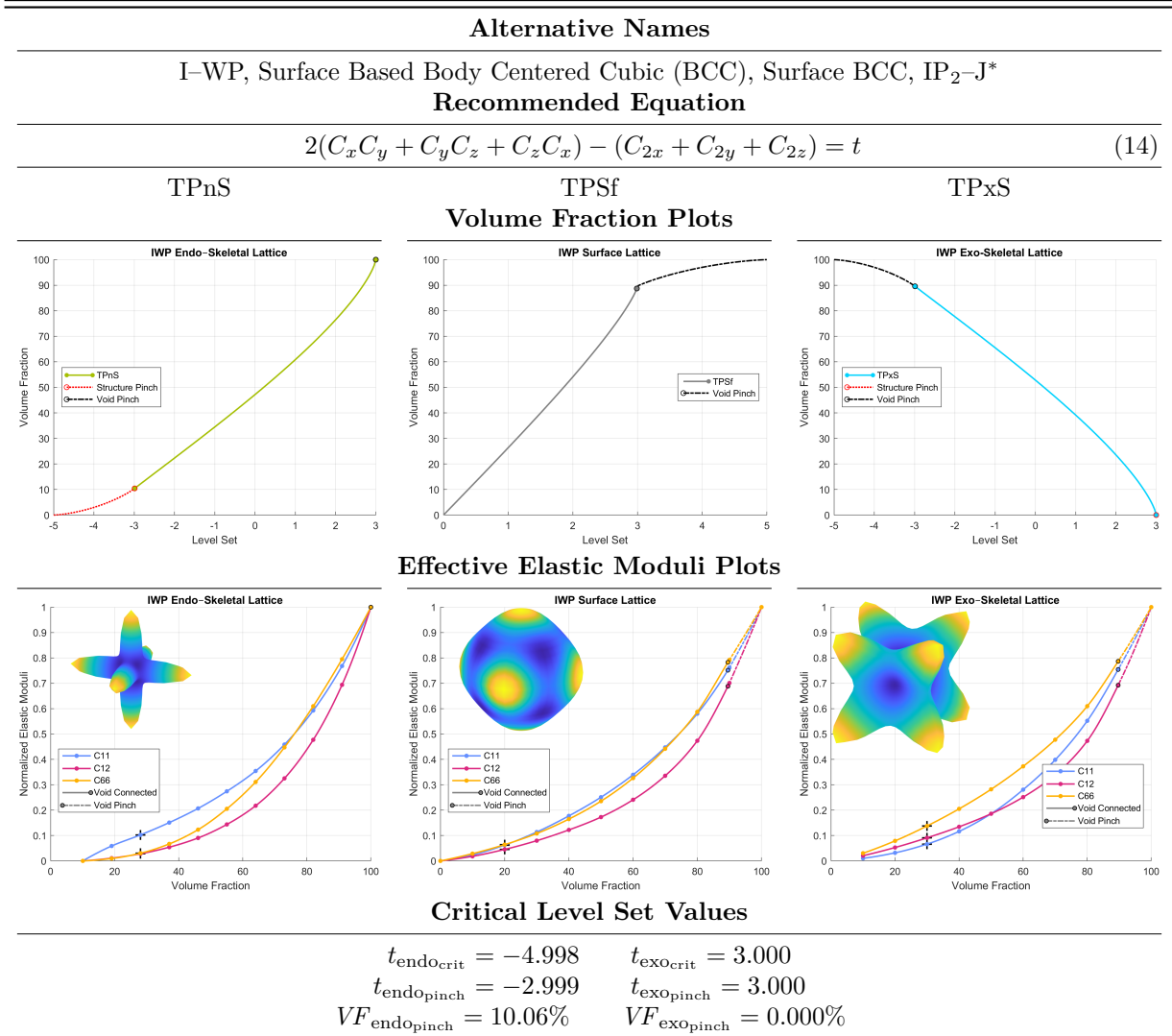


Figure 1 shows that when generating the TPxS of the IWP using Eq. 14, there is not a pinch-off point as the volume fraction approaches zero. Practical limits on the minimum volume fraction would still be imposed by modeling, meshing, and manufacturing techniques employed.

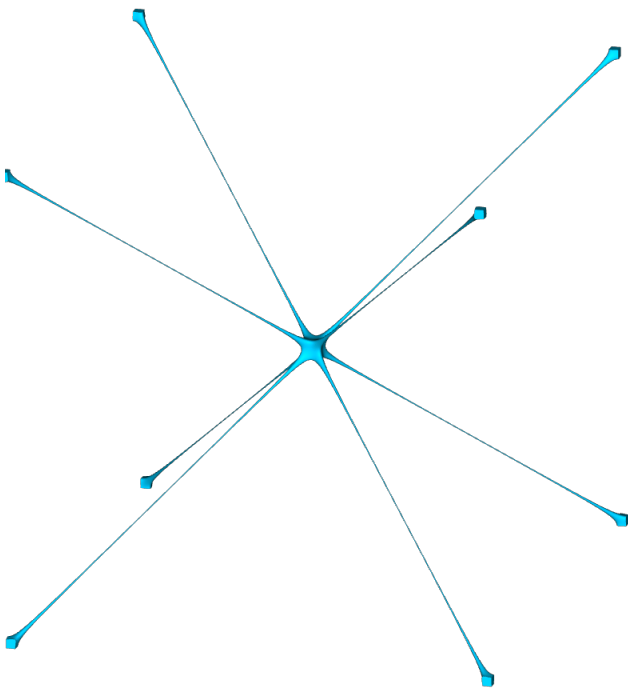


Figure 1: The TPxS of the IWP at a volume fraction of 0.0002 (0.2%) demonstrates that connectivity remains as the volume fraction approaches zero.

Remainder of page intentionally left blank

2.5 Neovius

Table 6: Summary for the Neovius Surface

Alternative Names	
$C_9(P)$, $C(P)$, Complementary P , P^*J^*	
Recommended Equation	
$3(C_x + C_y + C_z) + 4C_xC_yC_z = t$	
(15)	
TPnS/TPxS	TPSf
Volume Fraction Plots	
Effective Elastic Moduli Plots	
Critical Level Set Values	
$t_{\text{crit}} = \pm 13.000$ $t_{\text{pinch}} = \pm 0.749$ $VF_{\text{skel,pinch}} = 33.57\%$	

von Schnerring and Nesper (1991) presents the same equation for approximating the Neovius Surface but without the coefficient of 3 in front of the first term. This alternative equation produces geometry that differs significantly from the TPMS shown in Table 35. The geometry does, however, have the same general shape and is topologically homeomorphic with geometry generated with Eq. 15.

2.6 C(Y)

Table 7: Summary for the C(Y) surface

Alternative Names	
Fisher–Koch C(Y), Complementary Y, $(YY_{xxx})^*$	
Recommended Equation	
$-S_x S_y S_z + S_{2x} S_y + S_{2y} S_z + S_x S_{2z} - C_x C_y C_z + S_{2x} C_z + C_x S_{2y} + C_y S_{2z} = t$	(16)
TPnS/TPxS	TPSf
Volume Fraction Plots	
Effective Elastic Moduli Plots	
Critical Level Set Values	
$t_{\text{crit}} = \pm 3.535$ $t_{\text{pinch}} = \pm 1.835$ $VF_{\text{skel}_{\text{pinch}}} = 7.637\%$	
$t_{\text{pinch}2} = \pm 1.957$ $VF_{\text{skel}_{\text{pinch}2}} = 1.189$	

The lattices of C(Y) surface generated from Eq. 16 have a unique property (that is also seen in the C(D), D', and C(G) lattices) where, as the magnitude of the level set increases, the surface pinches off in such a way that there still exists a connected structure that spans the domain but with additional disconnected “floating” volumes also. The disconnected volumes can be removed from the lattice allowing for lattices to be generated from this approximation at a broader range of volume fractions. This is shown in Fig. 2 for the

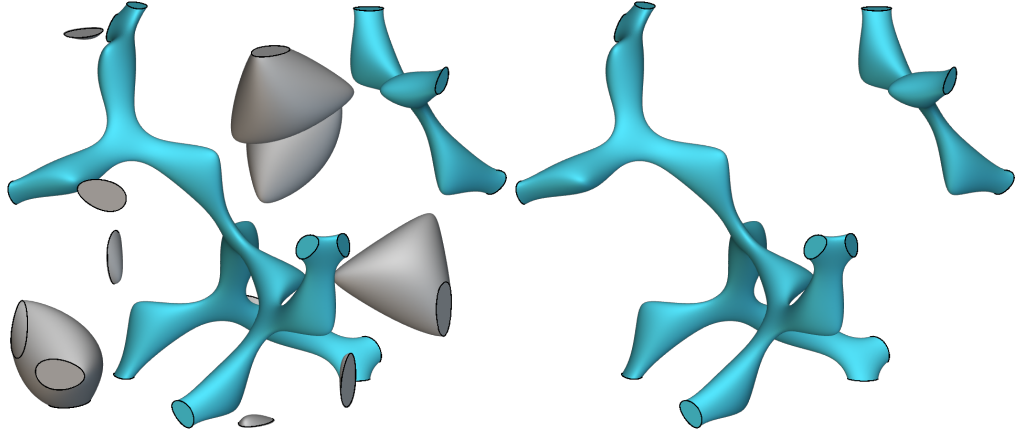


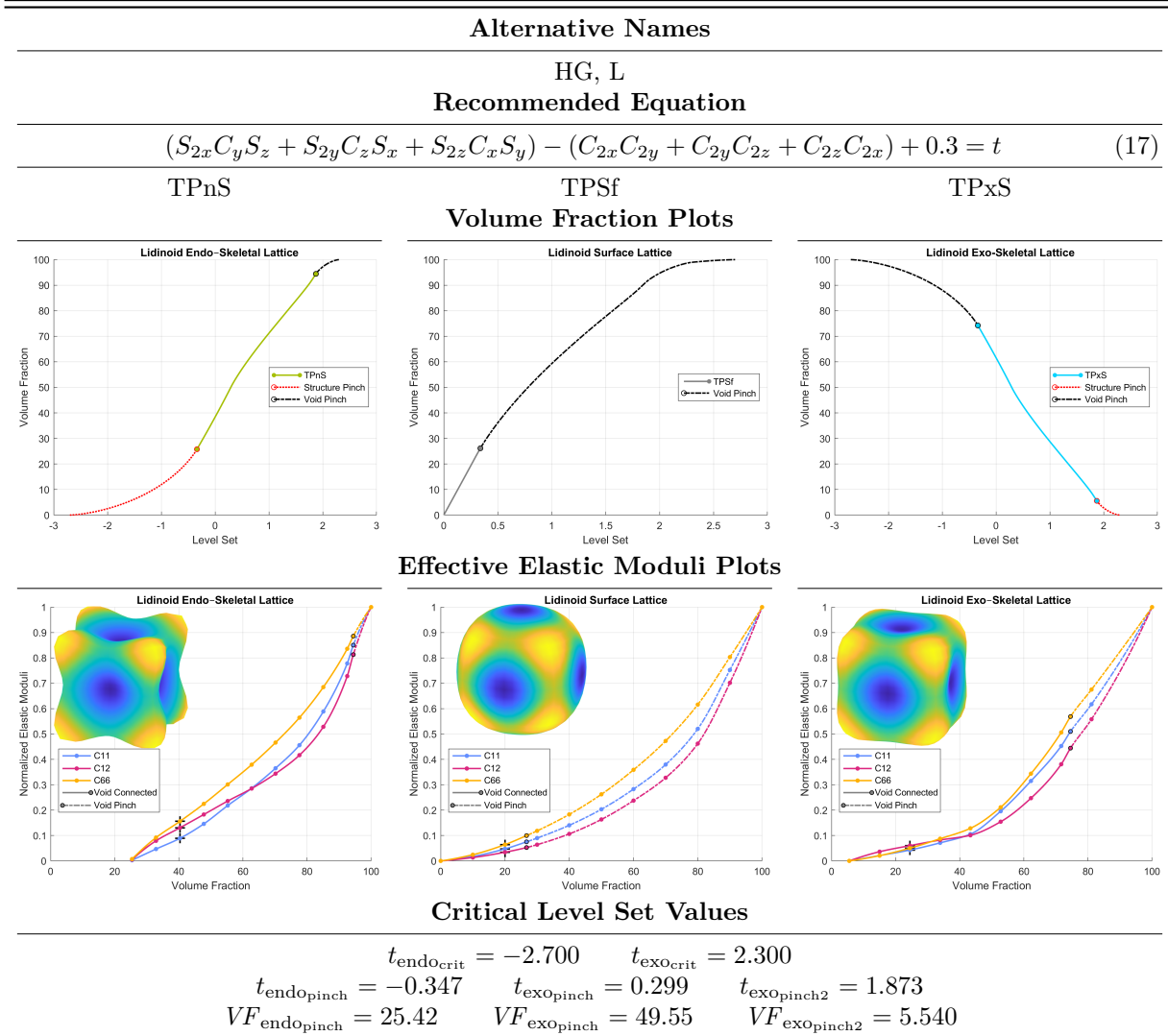
Figure 2: (left) Example of TPxS of the C(Y) surface at a level set value of $t = 1.9$ which falls between the two upper pinch level set values. Resulting in discontinuous sections, a connected lattice structure (right), and the same structure with discontinuous sections removed.

TPxS of the C(Y) surface. It is important to note that the connectivity of the lattice changes significantly when this happens and a large step change in the properties is likely also. For the C(Y) surface, it maintains some connectivity until secondary level sets of $t_{\text{exo}_{\text{pinch}2}} = 1.957$ or $t_{\text{endo}_{\text{pinch}2}} = -1.957$, with a volume fraction as low as $VF_{\text{exo}_{\text{pinch}2}} = 1.189$ or $VF_{\text{endo}_{\text{pinch}2}} = 1.189$ with the “floating” material removed. The pinching behavior of this surface differs from the Lidinoid, Split-P, G', and G'_2 surfaces which separate into finite numbers of connected structures (without “floating” volumes) between their respective first and second pinch level sets.

Remainder of page intentionally left blank

2.7 Lidinoid

Table 8: Summary for the Lidinoid Surface



Discovered by Sven Lidin in 1990 who referred to the surface as the HG surface (Lidin and Larsson, 1990). Equation 17 also appears in literature with the equation multiplied by a factor of one half (Wohlgemuth et al., 2001). Both produce the same surface approximation with the only functional change being that the value of t needed to produce a given offset is also halved.

$$\frac{1}{2}(S_{2x}C_yS_z + S_{2y}C_zS_x + S_{2z}C_xS_y) - \frac{1}{2}(C_{2x}C_{2y} + C_{2y}C_{2z} + C_{2z}C_{2x}) + 0.15 = t \quad (18)$$

The Lidinoid lattices have two upper pinch off points, an uncommon property seen also in the Split-P, G', and G'_2 Lattice. The first occurs at $t = 0.299$ and results in the TPxS pinching off into two bodies, that each span the domain⁴ until the second pinch-off point at $t = 1.873$. The TPxS of the Lidinoid is shown in Fig. 3 for three volume fractions below, between, and above the two pinch-off points. We note the existence of the first pinch-off point, even though the structures span the domain because the change in topology has an impact on the properties of the TPxS lattice, which can be seen in Table 8.

⁴ They connect to adjacent unit cells and can therefore fill a given domain with a connected structure.

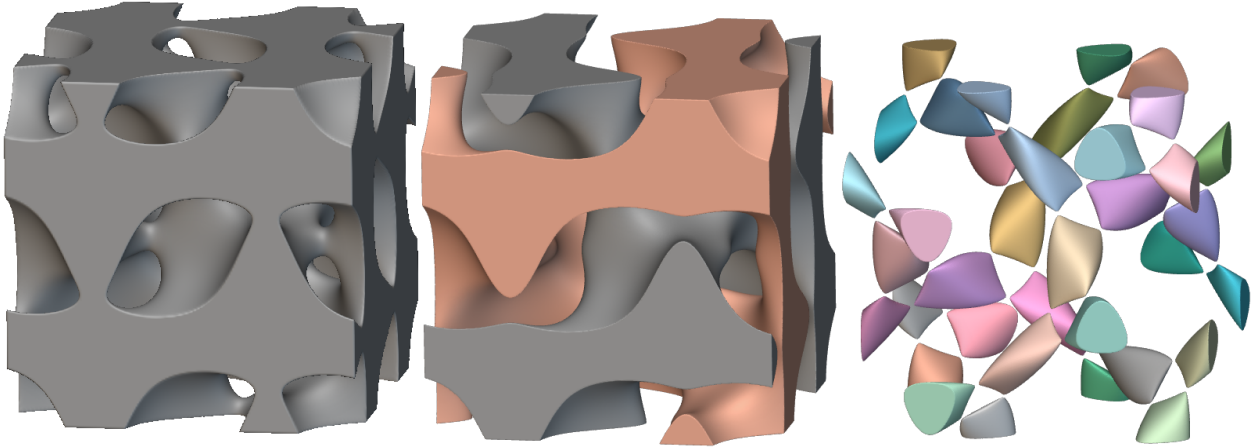
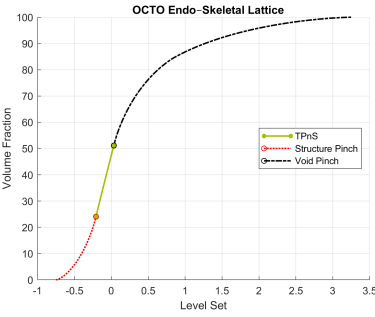
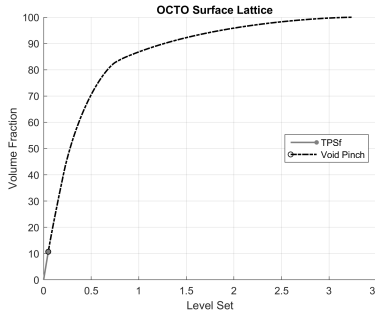
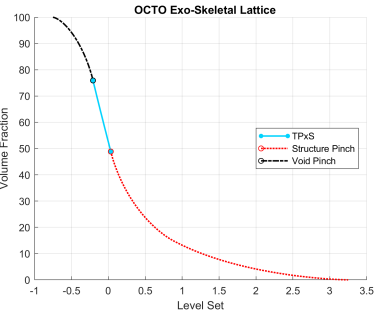
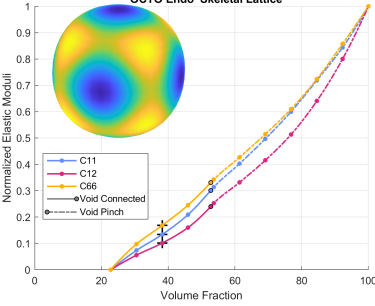
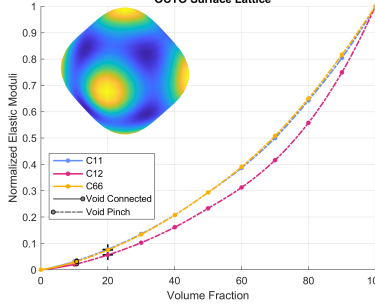
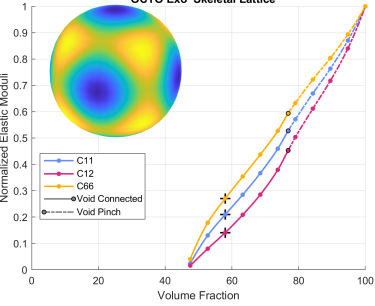


Figure 3: From left to right, the TPxS of the Lidinoid at level sets of 0.2, 0.4, and 1.875 which occur below $t_{\text{exo}_{\text{pinch}}}$, between $t_{\text{exo}_{\text{pinch}}}$ and $t_{\text{exo}_{\text{pinch}2}}$, and above $t_{\text{exo}_{\text{pinch}2}}$ respectively. Note that below $t_{\text{exo}_{\text{pinch}}}$, the TPxS is a single connected structure, between $t_{\text{exo}_{\text{pinch}}}$ and $t_{\text{exo}_{\text{pinch}2}}$ the TPxS is two separate structures that span the domain with one highlighted in orange. Above $t_{\text{exo}_{\text{pinch}2}}$ the TPxS is discontinuous.

Remainder of page intentionally left blank

2.8 OCTO

Table 9: Summary for the OCTO Surface

Alternative Names	
O,C–TO Recommended Equation	$0.6(C_x C_y + C_y C_z + C_z C_x) - 0.4(C_x + C_y + C_z) + 0.25 = t$ (19)
TPnS	TPSF
TPxS	
Volume Fraction Plots	
	
	
Effective Elastic Moduli Plots	
	
	
Critical Level Set Values	
$t_{\text{endo}_{\text{crit}}} = -0.750$	$t_{\text{exo}_{\text{crit}}} = 3.249$
$t_{\text{endo}_{\text{pinch}}} = -0.216$	$t_{\text{exo}_{\text{pinch}}} = 0.049$
$VF_{\text{endo}_{\text{pinch}}} = 22.75$	$VF_{\text{exo}_{\text{pinch}}} = 47.49$

Three different equations for fitting the OCTO surface (including Eq. 19) have been presented in literature and online sources. They all take the form of Eq. 20 and Table 10 presents the values of coefficients A , B , C , and t_0 used in the different approximations with the related source. Each is discussed and then compared to determine that Eq. 19 is preferred.

$$A(C_x C_y + C_y C_z + C_z C_x) + B(C_x + C_y + C_z) + C(C_x C_y C_z) + t_0 = t \quad (20)$$

Hsieh and Valdevit (2020) cites Wohlgemuth et al. (2001), but they change the value of the initial level set t_0 from 1 to 0.25. This applies a linear shift to the relationship between the applied level set and volume fraction for the different lattices generated, however, it does not truly change the underlying implicit equation. A t_0 value of 0.25 results in a surface that resembles the OCTO surface, whereas a value of 1 results in a surface that is offset to nearly the upper critical limit. Therefore, we use a value of 0.25 in our comparison. Changes to the ratio of the other coefficients do impact the geometry of the lattice structures.

Hoffman et al. (2003b) offers two equations for the OCTO surface (one using an additional term) in the approximation derived from different parameter families as presented in Wohlgemuth et al. (2001). Which

we find odd because that paper itself has a different equation from those presented online by the same group/author.

Table 10: Table of values presented for Eq. 19

A	B	C	t_0	Source
0.6	-0.4	0	0.25	Hsieh and Valdevit (2020)
4	-3	0	2.4	Hoffman et al. (2003b)
4	-2.8	1	1.5	Hoffman et al. (2003b)

To determine which equation best fits the surface, the unsigned Hausdorff Distance was computed using high-resolution meshes of: (1) the evolved surface representing the “true” minimal surface from Surface Evolver, and (2) the lattices implemented from nTopology. The results of these comparisons are summarized in Table 11 for a unit cell of size 1. The signed Hausdorff Distance is presented in Fig. 4 as well as in the database as .3mf files of the “true” surface overlaid with color indicating the relative distance from the “true” surface for each approximation.

Table 11: Statistics for normalized unsigned Hausdorff Distance for the three approximations of the OCTO surface. The first column shows the least deviation from the “truth” surface generated using Surface Evolver.

	Hsieh	MSRI_4_3_2.4	MSRI_4_2.8_1.5
min	0.000000	0.000000	0.000000
max	0.034956	0.052283	0.045158
mean	0.014993	0.022497	0.017603
RMS	0.016833	0.025693	0.020920

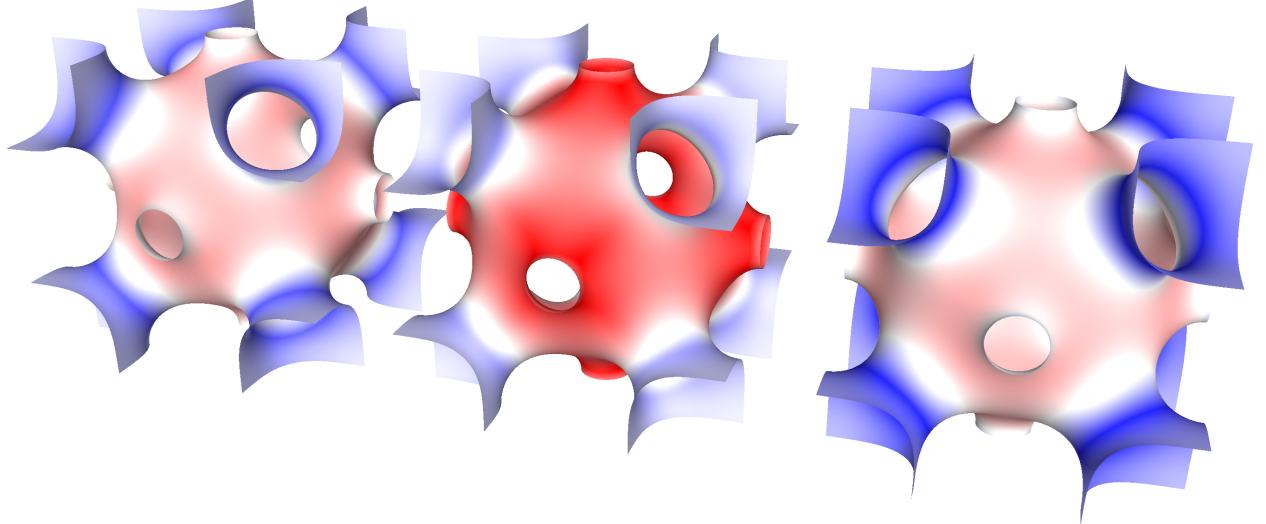


Figure 4: Signed Hausdorff Distance visualized by over plotting the distance on the “true” surface for each approximation the rows of Table 10 top to bottom relating to appearance left to right. Blue and red respectively show positive and negative distances from the “true” surface, based on the sign convention of the approximate equations, with greater intensity indicating greater distance. White is little to no difference between the two surfaces.

The coefficients used in Hsieh and Valdevit (2020) result in the least deviation from the OCTO surface generated by Surface Evolver. However, the other parameterizations offer a unique feature where the connectivity near the corners of the unit cell is broken at a different level set value from those at the face centers

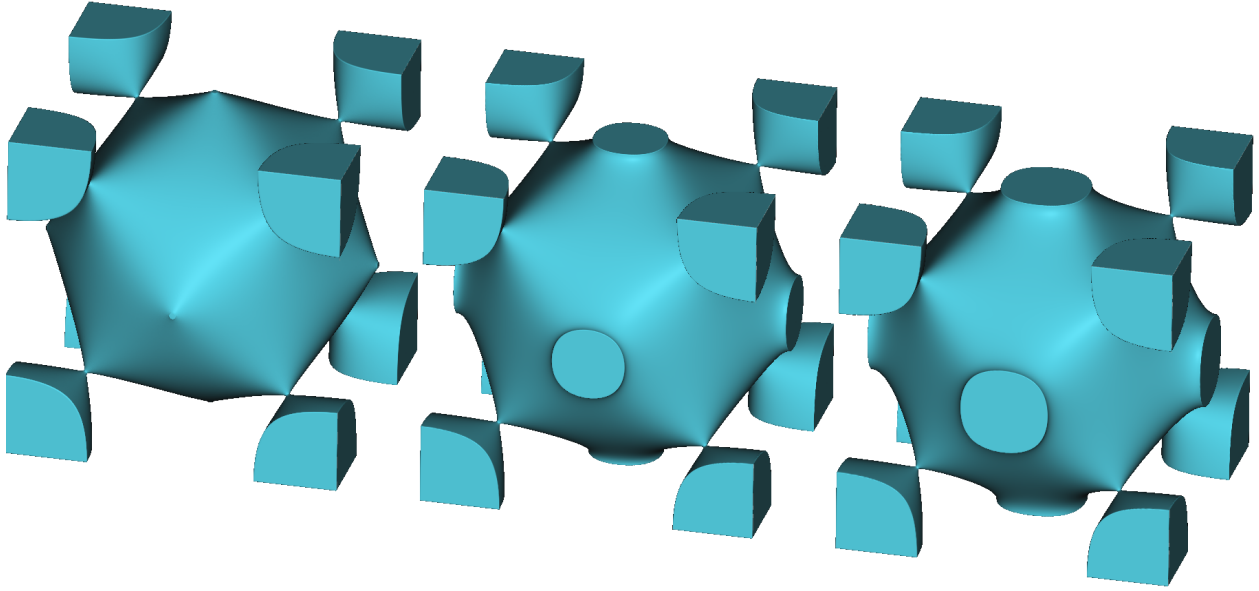


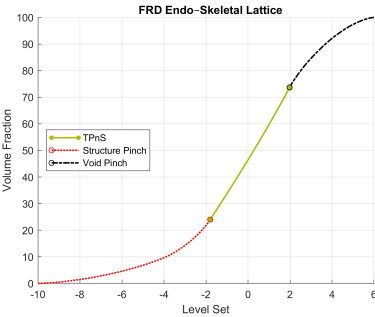
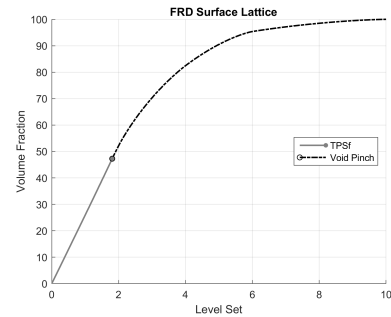
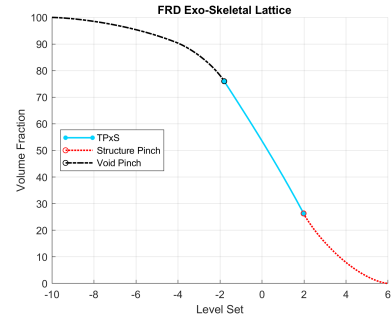
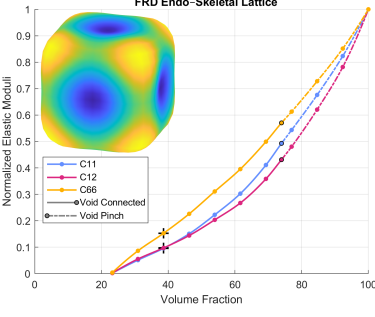
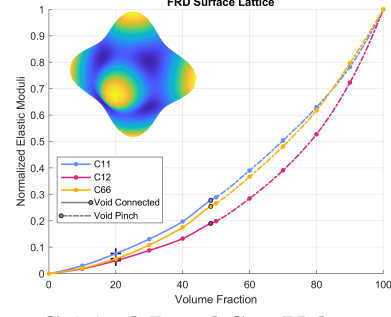
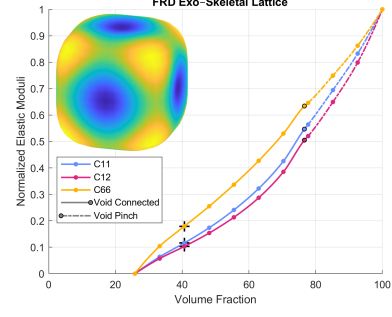
Figure 5: The TPxS of the OCTO surface, pinching off near the cell corners as at $t_{\text{endo}_{\text{pinch}}}$, using the three different parameterizations presented in [Table 10](#) with the rows top to bottom relating to appearance left to right.

of the cell, which can be seen in [Fig. 5](#). A comparison of the properties of the lattices generated by these different parameterizations is motivated.

Remainder of page intentionally left blank

2.9 FRD

Table 12: Summary for the FRD Surface

Alternative Names	
F-RD, $F_{xx}-P_2F_z$	
Recommended Equation	
$8C_xC_yC_z + C_{2x}C_{2y}C_{2z} - (C_{2x}C_{2y} + C_{2y}C_{2z} + C_{2z}C_{2x}) = t$ (21)	
TPnS  TPSf  TPxS 	
Volume Fraction Plots	
  	
Effective Elastic Moduli Plots	
Critical Level Set Values	
$t_{\text{endo}_{\text{crit}}} = -10.00$	$t_{\text{exo}_{\text{crit}}} = 6.000$
$t_{\text{endo}_{\text{pinch}}} = -1.851$	$t_{\text{exo}_{\text{pinch}}} = 1.999$
$VF_{\text{endo}_{\text{pinch}}} = 23.27$	$VF_{\text{exo}_{\text{pinch}}} = 25.84$

Equation 21 is take from Wohlgemuth et al. (2001) and also Hoffman et al. (2003b) (multiplied by a constant factor of 10). Hoffman et al. (2003b) presents a second equation for the FRD surface that is used in Hsieh and Valdevit (2020) without the second term and a different first coefficient:

$$4C_xC_yC_z - (C_{2x}C_{2y} + C_{2y}C_{2z} + C_{2z}C_{2x}) = t \quad (22)$$

The two different equations for the FRD surface were compared and it was determined that Eq. 21 offers a better fitting of the TPMS using the techniques discussed in Section 2.8 (with results in Table 13).

Table 13: Statistics for normalized unsigned Hausdorff Distance for the two approximations of the FRD surface. The second column shows a negligibly higher maximum distance, however, significantly better mean and RMS distance from the “truth” surface generated using Surface Evolver.

	2 Term	3 Term
min	0.000003	0.000000
max	0.012257	0.012326
mean	0.007706	0.003986
RMS	0.008414	0.004795

The FRD surface is sometimes shown with a smaller unit cell that is one octant (1/8th) of the unit cell shown in [Table 35](#). The smaller unit cell captures all of the unique geometry of the FRD surface, but requires rotation or mirroring to extend the lattice, whereas this larger unit cell is periodic.

Remainder of page intentionally left blank

2.10 S

Table 14: Summary for the S Surface

Alternative Names	
Fisher–Koch S, S*	
Recommended Equation	
$C_{2x}S_yC_z + C_xC_{2y}S_z + S_xC_yC_{2z} = t$	(23)
TPnS/TPxS	TPSf
Volume Fraction Plots	
Effective Elastic Moduli Plots	
Critical Level Set Values	
$t_{\text{crit}} = \pm 1.414$ $t_{\text{pinch}} = \pm 0.794$ $VF_{\text{skel,pinch}} = 11.48\%$	

2.11 P+C(P)

Table 15: Summary for the P+C(P) Surface

Alternative Names	
PN Recommended Equation	
$0.3(C_x C_y C_z) + 0.2(C_x + C_y + C_z) + 0.1(C_{2x} C_{2y} C_{2z}) + 0.1(C_{2x} + C_{2y} + C_{2z}) + 0.05(C_{3x} + C_{3y} + C_{3z}) + 0.1(C_x C_y + C_y C_z + C_z C_x) = t$ (24)	
TPnS	TPSf
Volume Fraction Plots	
Effective Elastic Moduli Plots	
Critical Level Set Values	
$t_{\text{endo}_{\text{crit}}} = -0.415$	$t_{\text{exo}_{\text{crit}}} = 1.750$
$t_{\text{endo}_{\text{pinch}}} = -0.134$	$t_{\text{exo}_{\text{pinch}}} = 0.174$
$VF_{\text{endo}_{\text{pinch}}} = 41.29$	$VF_{\text{exo}_{\text{pinch}}} = 21.74$

Although this surface's name might imply that it is an addition of the approximate equations of the P and Neovius (C(P)) surfaces, it is in fact a minimal surface discovered by Karcher (1989, p. 349). Likely for similar reasons, it is also referred to as the PN Surface by Hoffman et al. (2003b).

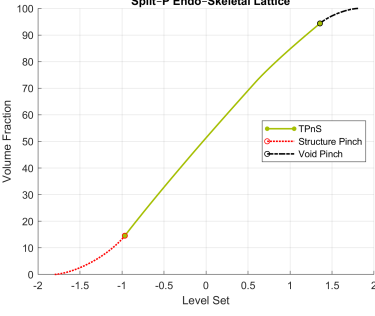
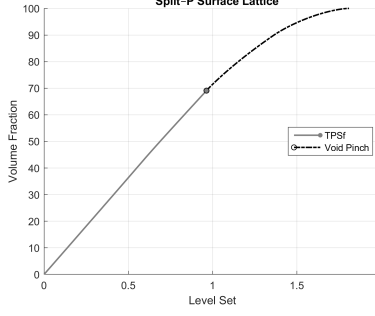
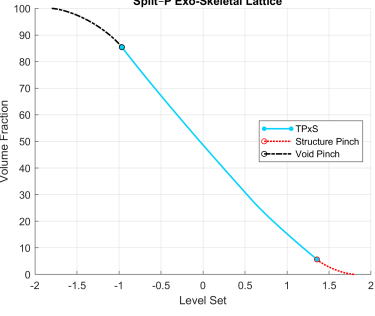
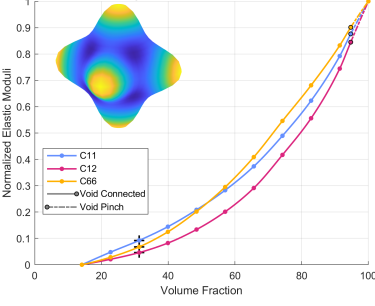
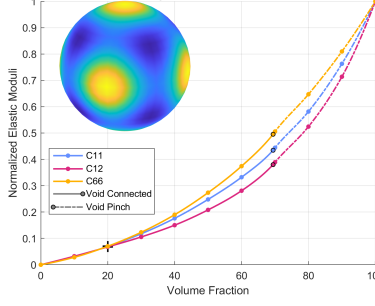
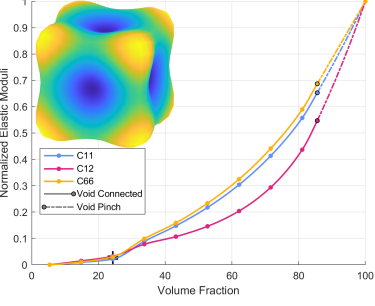
Two equations for the P+C(P) surfaces were found. Hoffman et al. (2003b) has Eq. 24 as shown, and Wohlgemuth et al. (2001) has the same, but with the first two coefficients of 0.3 and 0.1 changed to 0.35 and 0.2 respectively. As there was no Surface Evolver file available for this surface, we could not perform the same type of best-fit assessment used with the OCTO and FRD surfaces. We instead compare the mean curvature of the two versions. As demonstrated in Fisher et al. (2022), the mean curvature of an implicitly defined equation, like those presented here to approximate TPMS, can be determined analytically (Goldman, 2005). The resulting equation for the mean curvature is a field that can be used to find the mean curvature at any given level set. In this case, we are interested in a level set of zero. The minimum and maximum mean curvature on the surface can be found and, by point-wise and integration methods, the average value of the mean curvature on the surface can be computed. The surface that is closer to a minimal surface, which has zero mean curvature at all points, would have the smallest magnitude average,

minimum, and maximum mean curvature. Applying this methodology to the P+C(P), we find that the average, minimum, and maximum mean curvature of Eq. 24 are closer to zero when the coefficients, 0.3 and 0.1 are used compared to the coefficients 0.35 and 0.2.

Remainder of page intentionally left blank

2.12 Split-P

Table 16: Summary for the Split-P Surface

Alternative Names	
P2-DG Recommended Equation	
$1.1(S_{2x}C_yS_z + S_{2y}C_zS_x + S_{2z}C_xS_y) - 0.2(C_{2x}C_{2y} + C_{2y}C_{2z} + C_{2z}C_{2x}) - 0.4(C_{2x} + C_{2y} + C_{2z}) = t \quad (25)$	
TPnS	TPSf
	Volume Fraction Plots
	
	TPxS
	
Effective Elastic Moduli Plots	
	
	Split-P Exo-Skeletal Lattice
	
Critical Level Set Values	
$t_{\text{endo}_{\text{crit}}} = -1.800$	$t_{\text{exo}_{\text{crit}}} = 1.810$
$t_{\text{endo}_{\text{pinch}}} = -0.969$	$t_{\text{exo}_{\text{pinch}}} = 0.599$
$VF_{\text{endo}_{\text{pinch}}} = 14.15$	$VF_{\text{exo}_{\text{pinch}}} = 27.58$
	$t_{\text{exo}_{\text{pinch2}}} = 1.370$
	$VF_{\text{exo}_{\text{pinch2}}} = 5.367$

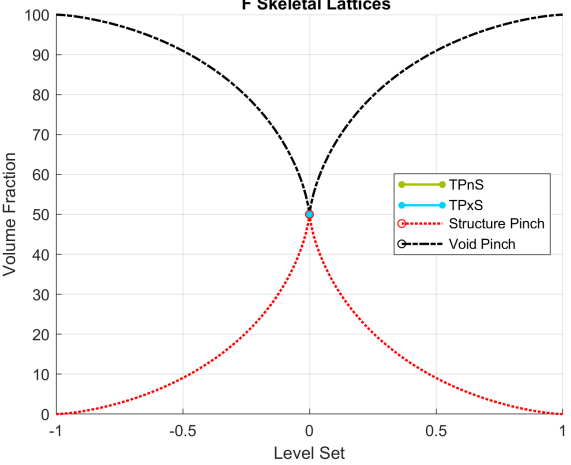
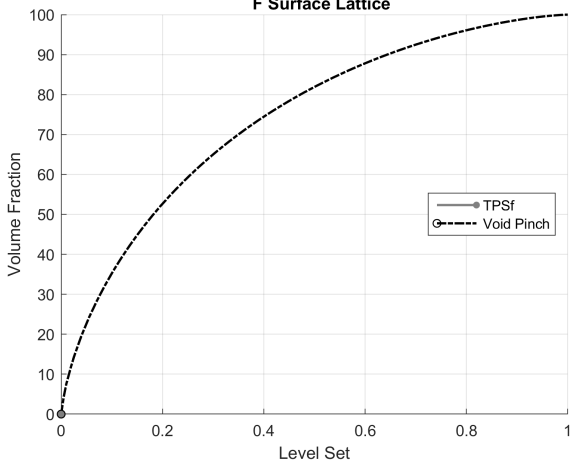
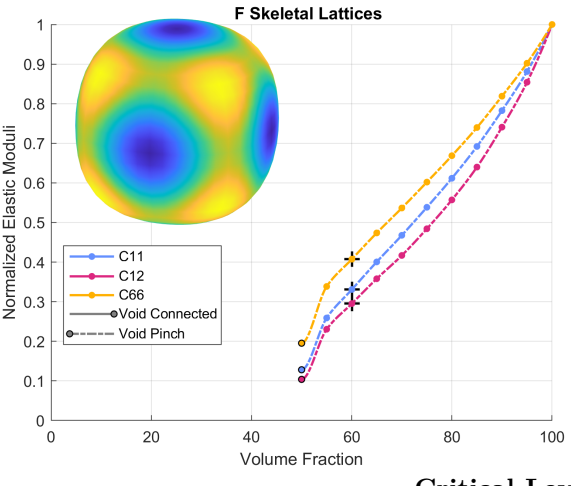
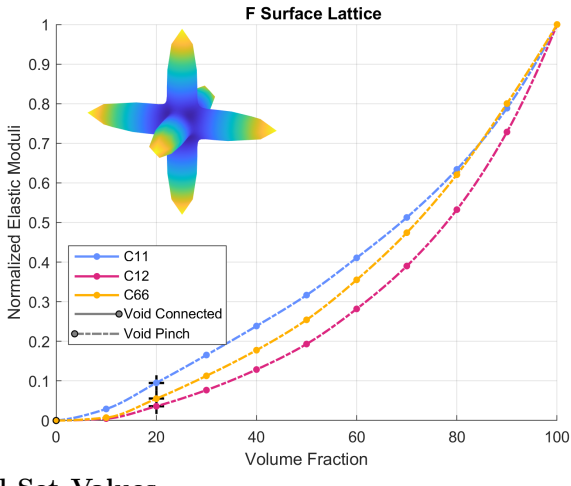
Equation 25 is taken from Hoffman et al. (2003a). This surface is also found in Wohlgemuth et al. (2001) with an equation that, when multiplied by two, is the same except for a different coefficient for the first term 1.4 vs 1.1. Performing the analysis outlined in Section 2.11, we selected a coefficient of 1.1 because it leads to a smaller average, maximum, and range of mean curvatures.

The equation for the Split-P surface was first derived by the addition of the equations of the Double Gyroid (Section 2.28) and the P (Section 2.3) surfaces (Wohlgemuth et al., 2001). Although we are not aware of a defined TPMS that relates to the Split-P equation, it is included here as it exhibits similar curvature properties and can be implemented in the same way as those that approximate a TPMS.

The Split-P lattices have two upper pinch-off points, an uncommon property seen also in the Lidinoid, G', and G'_2 lattices. The first occurs at $t = 0.6$ and results in the TPxS pinching off into two bodies, that each span the domain until the second pinch-off point at $t = 1.37$. The effect of the two pinch-off points is shown for the Lidinoid surface in Fig. 3. We note the existence of the first pinch-off point, even though the structures span the domain because the change in topology has an impact on the properties of the TPxS lattice, which can be seen in the TPxS effective elastic moduli plot in Table 16.

2.13 F

Table 17: Summary for the F Surface

Alternative Names	
F^* , tripleplane1	
Recommended Equation	
	$C_x C_y C_z = t$ (26)
TPnS/TPxS	TPSf
Volume Fraction Plots	
	
Effective Elastic Moduli Plots	
	
Critical Level Set Values	
$t_{\text{crit}} = \pm 1.000$ $t_{\text{pinch}} = \pm 0.000$ $VF_{\text{skel,pinch}} = 50.00\%$	

The zero level set generated by Eq. 26 produces three sets of orthogonal planes whose normals are aligned with the x , y , and z axes with a spacing of $d_i/2$. As a result, as the level set approaches zero, the maximum and mean curvatures approach infinity at the intersection of any of the planes, and all curvatures approach zero away from the intersections. Per Lord and Mackay (2003), Eq. 26 is based on the second surface in a converging sequence of surfaces that approach three sets of orthogonal planes. The first six surfaces in

the sequence are visualized on [Brakke \(b\)](#) identified as “Triplane Surfaces” (the specific surface of interest is “Triplane1” based on file naming). [Equation 26](#) would be a better fit for a later member of the sequence of surfaces, but doesn’t capture the “tunnels” through the surface that let it approach the orthogonal planes without intersecting and still maintain zero mean curvature.

The TPnS and TPxS are connected only for $VF > 0.5$. As a result, regardless of which of the three lattices are generated, there will always be closed internal regions. The number of regions will be double for the TPSf because it will have regions associated with both the TPnS and TPxS. As a result, F lattices would not be suitable for AM processes where overhangs are not possible (e.g. Material Jetting) or processes where feed material would be trapped (e.g. Powder Bed Fusion, or Vat Photopolymerization). The trapped feed material can be avoided if the closed internal regions are connected by cutting holes in the lattice.

Remainder of page intentionally left blank

2.14 C(D)

Table 18: Summary for the C(D) Surface

Alternative Names	
C(D*), Complementary D Recommended Equation	
$C_{3x+y}C_z - S_{3x-y}S_z + C_{x+3y}C_z + S_{x-3y}S_z + C_{x-y}C_{3z} - S_{x+y}S_{3z} = t$	(27)
TPnS/TPxS	TPSf
Volume Fraction Plots	
Effective Elastic Moduli Plots	
Critical Level Set Values	
$t_{\text{crit}} = \pm 4.250$ $t_{\text{pinch}} = \pm 0.158$ $VF_{\text{skel}_{\text{pinch}}} = 41.22\%$	
$t_{\text{pinch2}} = \pm 0.272$ $VF_{\text{skel}_{\text{pinch2}}} = 24.45$	

The approximation to the Complementary D surface, stylized as C(D) surface, in Eq. 27 is taken from von Schnering and Nesper (1991), which also presented a second equation (Eq. 28) for the C(D) surface.

$$C_{3x}C_yC_z - S_{3x}S_yS_z + C_xC_{3y}C_z - S_xS_{3y}S_z + C_xC_yC_{3z} - S_xS_yS_{3z} = t \quad (28)$$

von Schnering and Nesper (1991) state that this second equation models the topology shifted by $\pi/4$ (1/8 of a

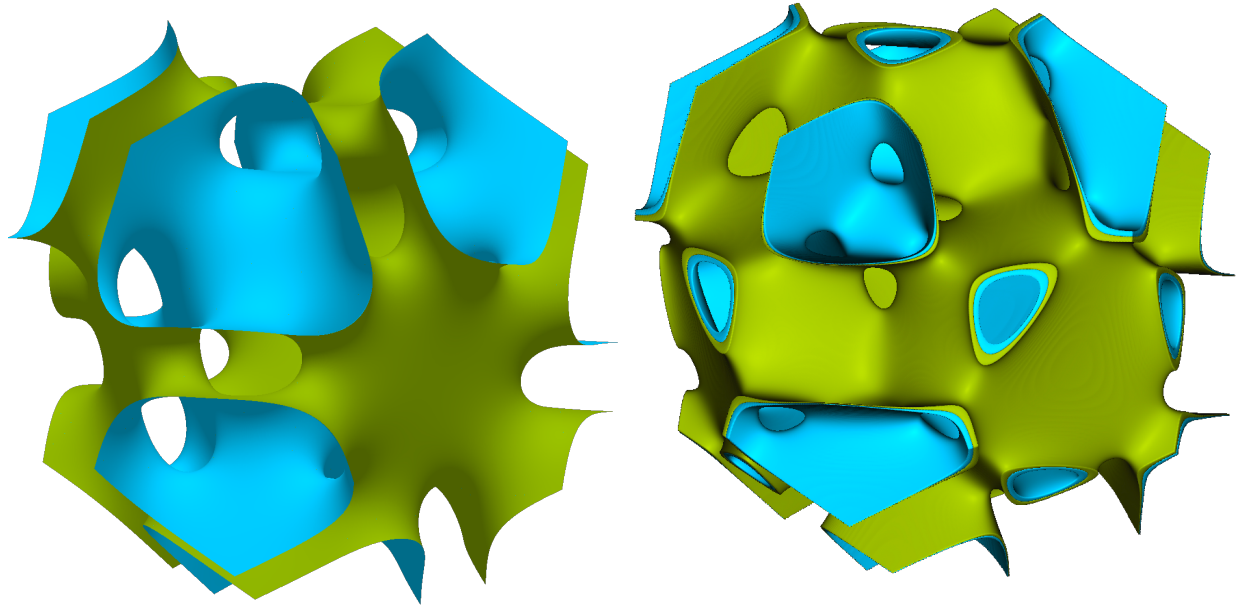


Figure 6: The C(D) surface generated in a rhombic dodecahedral domain using (left) Surface Evolver and (right) Eq. 27 in topology. Discrepancies between the intended surface from Surface Evolver and the approximate equation can be seen more clearly with this cut.

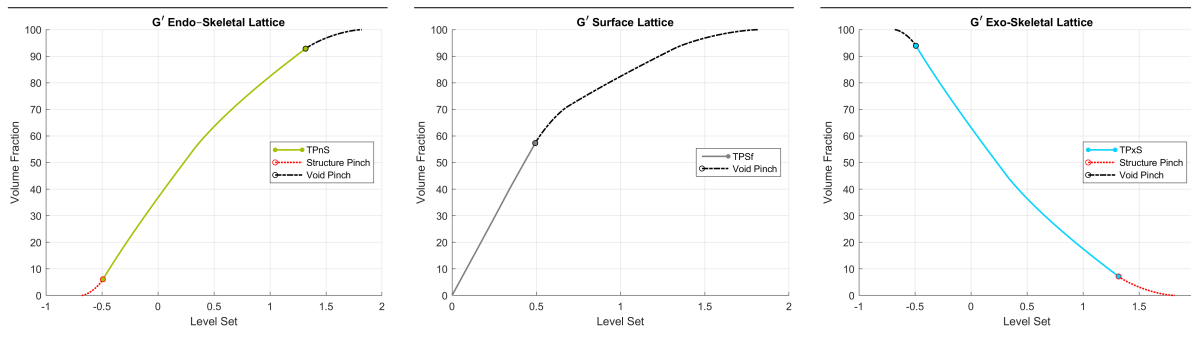
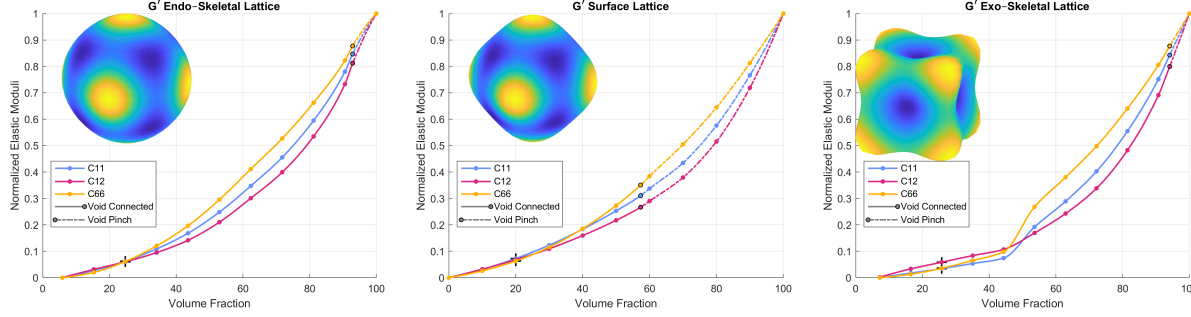
period) in x , y , and z . After accounting for the shift, at the same level set, we confirmed that, after accounting for the shift, the two equations produce functionally identical lattices with no discernible differences. We elect to implement Eq. 27 for consistency with Hsieh and Valdevit (2020). We have not explored if the relationship between level set and volume fraction is the same when implementing Eq. 27 vs. Eq. 28, and we only derive limits and relationships for Eq. 27.

When comparing the lattices produced using Eq. 27 to the TPMS as generated in Surface Evolver, a number of topological differences were found. To highlight this, the TPMS and TPSf of the C(D) surface were modeled in rhombic dodecahedral domains (see Fig. 6). Additional connections can be seen in the lattice that are not present in the TPMS; however, we are not aware of any alternative equations that more closely model the TPMS.

The lattices of C(D) surface generated from Eq. 27 have a unique property (that is also seen in the C(Y), D', and C(G) lattices) where, as the magnitude of the level set increases, the surface pinches off in such a way that there still exists a connected structure that spans the domain but with additional disconnected “floating” volumes also. The disconnected volumes can be removed from the lattice allowing for lattices to be generated from this approximation at a broader range of volume fractions. This is demonstrated in Fig. 2 with the TPxS of the C(Y) surface. It is important to note that the connectivity of the lattice changes significantly when this happens and a large step change in the properties is possible also. For the C(D) surface, it maintains some connectivity until secondary level sets of $t_{\text{exo}_{\text{pinch}_2}} = 0.272$ ($t_{\text{endo}_{\text{pinch}_2}} = -0.272$) and, a volume fraction as low as $VF_{\text{exo}_{\text{pinch}_2}} = 24.45$ with the “floating” material removed. The pinching behavior of this surface differs from the Lidinoid, Split-P, G', and G'_2 surfaces which separate into finite numbers of connected structures (without “floating” volumes) between their respective first and second pinch level sets.

2.15 G'

Table 19: Summary for the G' Surface

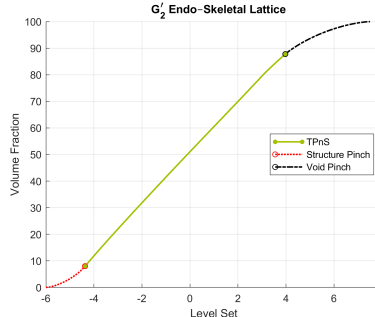
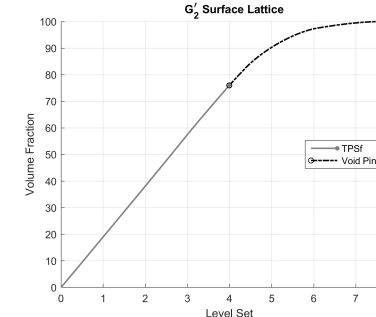
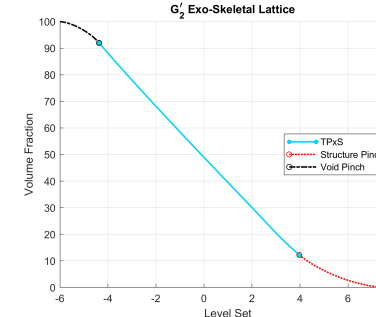
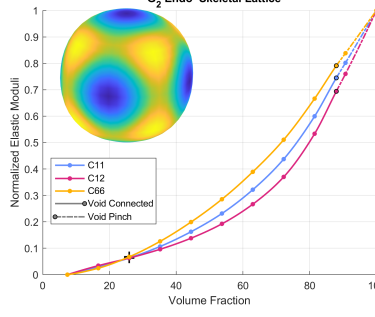
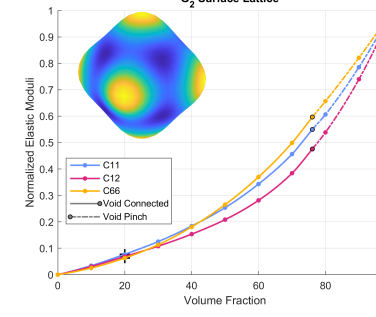
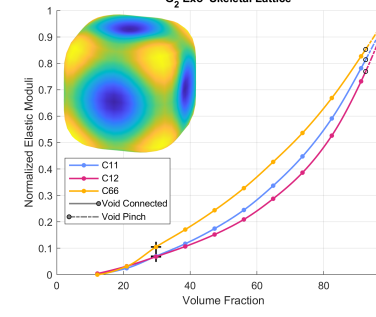
Alternative Names	
None Found	
Recommended Equation	
$S_{2x}C_yS_z + S_xS_{2y}C_z + C_xS_yS_{2z} + 0.32 = t$ (29)	
TPnS	TPSF
Volume Fraction Plots 	
Effective Elastic Moduli Plots 	
Critical Level Set Values $t_{\text{endo}_{\text{crit}}} = -0.680 \quad t_{\text{exo}_{\text{crit}}} = 1.820$ $t_{\text{endo}_{\text{pinch}}} = -0.494 \quad t_{\text{exo}_{\text{pinch}}} = 0.319 \quad t_{\text{exo}_{\text{pinch2}}} = 1.319$ $VF_{\text{endo}_{\text{pinch}}} = 5.896 \quad VF_{\text{exo}_{\text{pinch}}} = 45.03 \quad VF_{\text{exo}_{\text{pinch2}}} = 7.213$	

Two equations for the G' surface are given by Hoffman et al. (2003b): Eq. 29 which appears to be first defined in Wohlgemuth et al. (2001), and Eq. 30 for which the source is unknown. Equation 29 appears in the MiniSurf tool presented in (Hsieh and Valdevit, 2020) and Eq. 30, divided by a factor of five, appears in Karlsson et al. (2021), Strömberg (2021), Zeleny (2013). The geometry generated from Eq. 30 was sufficiently different to warrant its own discussion presented separately in Section 2.16 with the new name G'_2.

The G' lattices have two upper pinch-off points, an uncommon property seen also in the Lidinoid, Split-P, and G'_2 lattices. The first occurs at $t = 0.319$ and results in the TPxS pinching off into two bodies, that each span the domain until the second pinch-off point at $t = 1.319$. The effect of the two pinch-off points is shown for the Lidinoid surface in Fig. 3. We note the existence of the first pinch-off point, even though the structures span the domain because the change in topology has an impact on the properties of the TPxS lattice, which can be seen in Table 19.

2.16 G'_2

Table 20: Summary for the G'_2 Surface

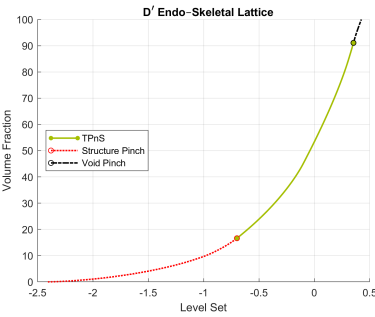
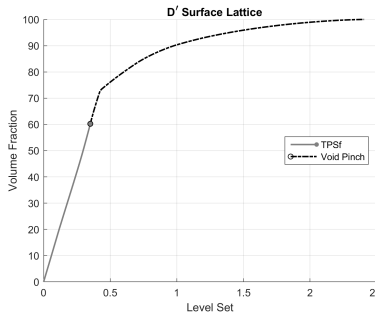
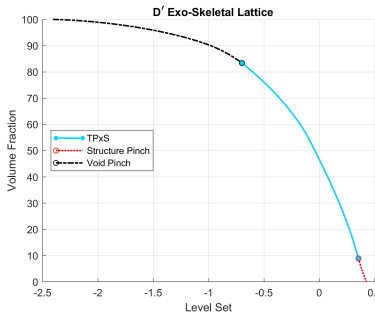
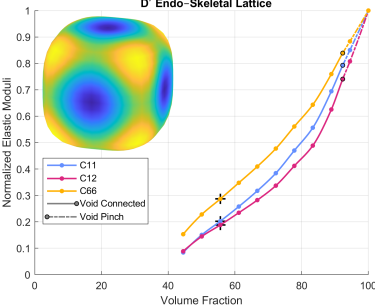
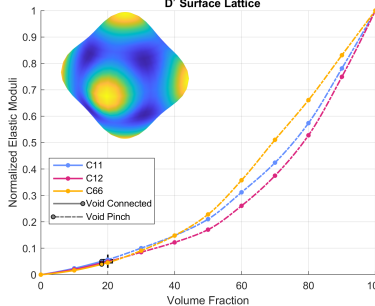
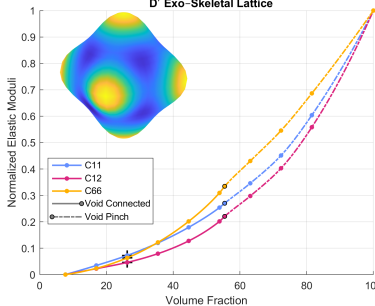
Alternative Names	
None Found	
Recommended Equation	
	$5(S_{2x}C_yS_z + S_xS_{2y}C_z + C_xS_yS_{2z}) + (C_{2x}C_{2y} + C_{2y}C_{2z} + C_{2z}C_{2x})$ (30)
TPnS	
TPSF	
Volume Fraction Plots	
	
	
Effective Elastic Moduli Plots	
	
	
Critical Level Set Values	
$t_{\text{endo}_{\text{crit}}} = -5.999$ $t_{\text{endo}_{\text{pinch}}} = -4.429$ $VF_{\text{endo}_{\text{pinch}}} = 7.400$	$t_{\text{exo}_{\text{crit}}} = 7.499$ $t_{\text{exo}_{\text{pinch}}} = 2.999$ $VF_{\text{exo}_{\text{pinch}}} = 20.55$
	$t_{\text{exopinch}_2} = 3.999$ $VF_{\text{exopinch}_2} = 12.18$

Equation 30 is the second equation for the G' surface given by Hoffman et al. (2003b), and is presented in this section. It has been given its own section because the geometry generated is sufficiently different. The name G'_2 was selected for lattice generated by Eq. 30 to differentiate them from the G' lattices but maintain a clear indicator that they are related in the literature. Equation 30 has the same form as Eq. 38 for the $C(I_2-Y^{**})$ surface with the first coefficient changed to 5. For the TPnS, the geometry generated by Eq. 29 and Eq. 30 has similar connectivity, but Eq. 30 is much closer in topology to Eq. 38. For the TPxS, the two approximations are significantly different, and further Eq. 30 exhibits significant differences also from Eq. 38 as the level set values move away from zero.

The G'_2 lattices have two upper pinch-off points, an uncommon property seen also in the Lidinoid, Split-P, and G' lattices. The first occurs at $t = 2.999$ and results in the TPxS pinching off into two bodies, that each span the domain until the second pinch-off point at $t = 3.999$. The effect of the two pinch-off points is shown for the Lidinoid surface in Fig. 3. We note the existence of the first pinch-off point, even though the structures span the domain because the change in topology has an impact on the properties of the TPxS lattice, which can be seen in Table 20.

2.17 D'

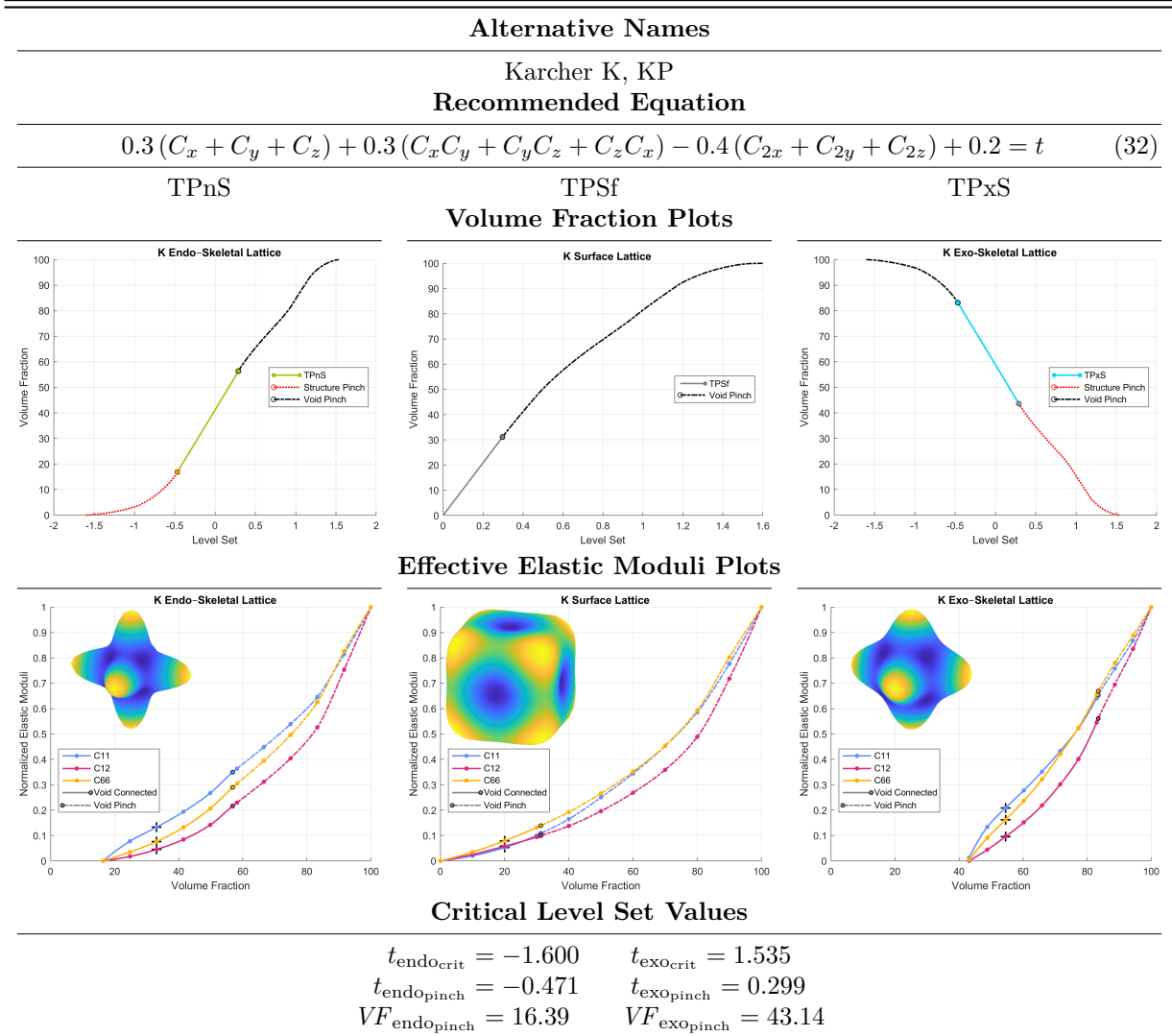
Table 21: Summary for the D' Surface

Alternative Names	
None Found	
Recommended Equation	
$\frac{1}{2}(C_x C_y C_z + C_x S_y S_z + S_x C_y S_z + S_x S_y C_z) - \frac{1}{2}(S_{2x} S_{2y} + S_{2y} S_{2z} + S_{2z} S_{2x}) - 0.2 = t \quad (31)$	
TPNs	TPSf
Volume Fraction Plots	
	
	
Effective Elastic Moduli Plots	
	
	
Critical Level Set Values	
$t_{\text{endo}_{\text{crit}}} = -2.406$	$t_{\text{exo}_{\text{crit}}} = 0.425$
$t_{\text{endo}_{\text{pinch2}}} = -0.699$	$t_{\text{endo}_{\text{pinch}}} = -0.106$
$VF_{\text{endo}_{\text{pinch2}}} = 15.43$	$VF_{\text{endo}_{\text{pinch}}} = 44.52$
	$VF_{\text{exo}_{\text{pinch}}} = 7.739$

The lattices of D' surface generated from Eq. 31 have a unique property (that is also seen in the C(Y), C(D), and C(G) lattices) where, as the level set becomes more negative, the surface pinches off in such a way that there still exists a connected structure that spans the domain but with additional disconnected “floating” volumes also. The disconnected volumes can be removed from the lattice allowing for lattices to be generated from this approximation at a broader range of volume fractions. This is demonstrated in Fig. 2 with the TPxs of the C(Y) surface. It is important to note that the connectivity of the lattice changes significantly when this happens and a large step change in the properties is likely also. For the C(D) surface, it maintains some connectivity until the secondary lower level set of $t_{\text{endo}_{\text{pinch2}}} = -0.699$ and, a volume fraction as low as $VF_{\text{endo}_{\text{pinch}}} = 15.43$ with the “floating” material removed. The pinching behavior of this surface differs from the Lidinoid, Split-P, G', and G'_2 surfaces which separate into finite numbers of connected structures (without “floating” volumes) between their respective first and second pinch level sets.

2.18 K

Table 22: Summary for the K Surface

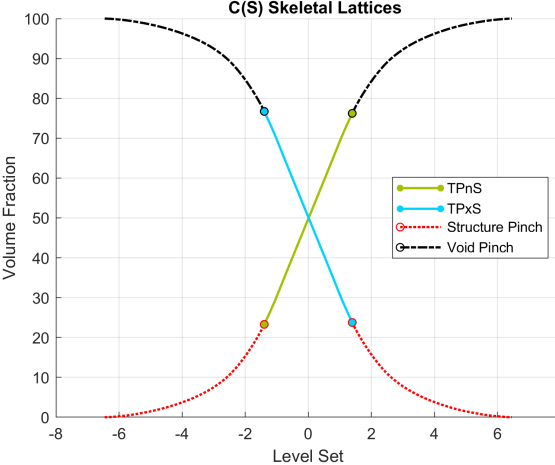
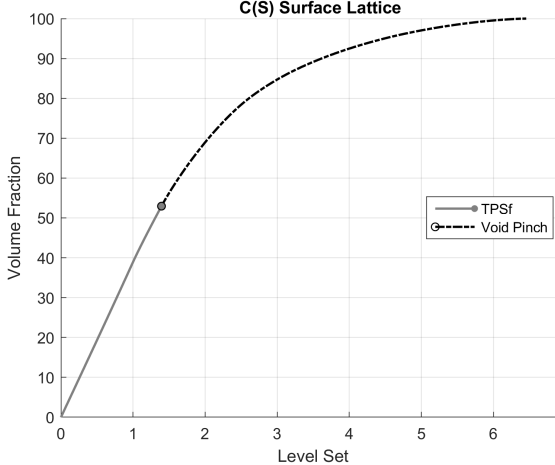
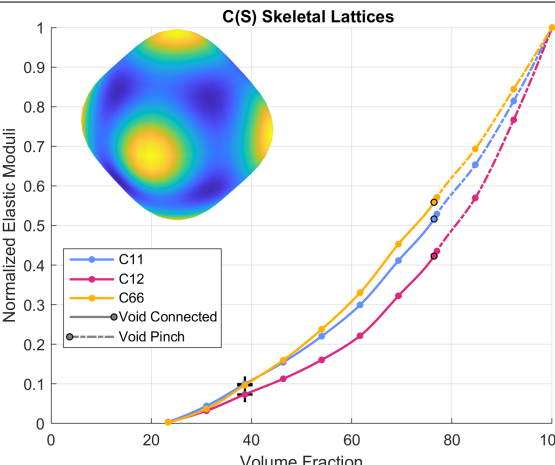
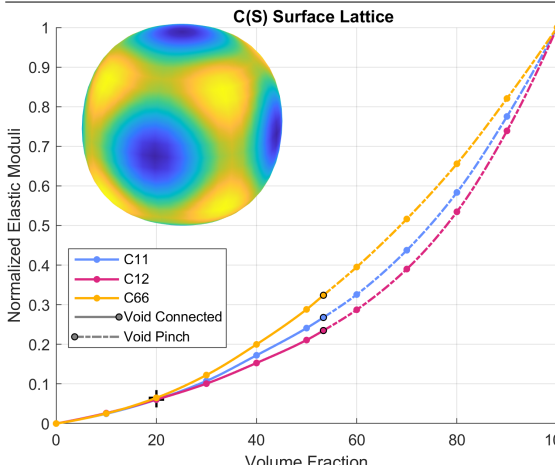


Hoffman et al. (2003b) presents another equation for this surface with slightly different coefficients and the third term changed to the product of the three C_{2i} terms rather than the sum. When generating the surface with this equation, a structure distinct from the K is produced and the change from a sum to a product is likely in error. To compare Eq. 32 against this second equation, we used the coefficients from the Hoffman et al. (2003b) equation and the third term as a sum, as shown in (Eq. 33). The two equations were compared using the methodology described in Section 2.11. We selected Eq. 32 because it leads to smaller average, minimum, and maximum mean curvatures.

$$0.6(C_x + C_y + C_z) + 0.7(C_x C_y + C_y C_z + C_z C_x) - 0.9(C_{2x} + C_{2y} + C_{2z}) + 0.4 \quad (33)$$

2.19 C(S)

Table 23: Summary for the C(S) Surface

Alternative Names	
Complementary S, Fisher–Koch C(S) Recommended Equation	
$(C_{2x} + C_{2y} + C_{2z}) + 2(S_{3x}S_{2y}C_z + C_xS_{3y}S_{2z} + S_{2x}C_yS_{3z}) + 2(S_{2x}C_{3y}S_z + S_xS_{2y}C_{3z} + C_{3x}S_yS_{2z}) = t$	(34)
TPnS/TPxS	TPSf
Volume Fraction Plots	
 <p>C(S) Skeletal Lattices</p>	 <p>C(S) Surface Lattice</p>
Effective Elastic Moduli Plots	
 <p>C(S) Skeletal Lattices</p>	 <p>C(S) Surface Lattice</p>
Critical Level Set Values	
$t_{\text{crit}} = \pm 6.455$ $t_{\text{pinch}} = \pm 1.407$ $VF_{\text{skel,pinch}} = 23.34\%$	

The Complementary S surface, stylized here as the C(S) surface was presented in Koch and Fischer (1988), was later determined to be identical to the P–surface (Koch and Fischer, 1993). However, the geometry generated by Eq. 34 for the C(S) surface, found in Hsieh and Valdevit (2020) and Michielsen and Kole (2003), is distinct from the P–surface (Section 2.3) and the geometry from Eq. 13. This can be seen by

comparing images of the P and C(S) lattices in [Table 35](#). Because the C(S) lattices are distinct from those of the P surface, they offer different properties and have been included in this dataset, even though they do not directly relate to a known TPMS. We considered alternative names for [Eq. 34](#) to help differentiate it from the defunct C(S) TMPS, but ultimately determined that changing the name could lead to further confusion.

Remainder of page intentionally left blank

2.20 Y

Table 24: Summary for the Y-Surface

Alternative Names	
Fisher–Koch Y	Recommended Equation
$C_x C_y C_z + S_x S_y S_z + (S_{2x} S_y + S_{2y} S_z + S_x S_{2z}) + (C_x S_{2y} + C_y S_{2z} + S_{2x} C_z) = t$	(35)
TPnS/TPxS	TPSf
Volume Fraction Plots	
Effective Elastic Moduli Plots	
Critical Level Set Values	
$t_{\text{crit}} = \pm 4.950$ $t_{\text{pinch}} = \pm 0.451$ $VF_{\text{skel,pinch}} = 25.80\%$	

The Y-surface was presented in Koch and Fischer (1988) but it was later determined that the Y-surface is identical to the D-surface (Koch and Fischer, 1993). However, the geometry generated by Eq. 34 for the Y-surface, found in Hsieh and Valdevit (2020) and Michielsen and Kole (2003), is distinct from the D-surface (Section 2.2) and the geometry from Eq. 12. This can be seen by comparing images of the D and Y lattices in Table 35. Because the Y lattices are distinct from those of the D-surface, they offer different properties

and have been included in this dataset, even though they do not directly relate to a known TPMS. We considered alternative names for Eq. 35 to help differentiate it from the defunct Y TMPS, but ultimately determined that changing the name could lead to further confusion.

Remainder of page intentionally left blank

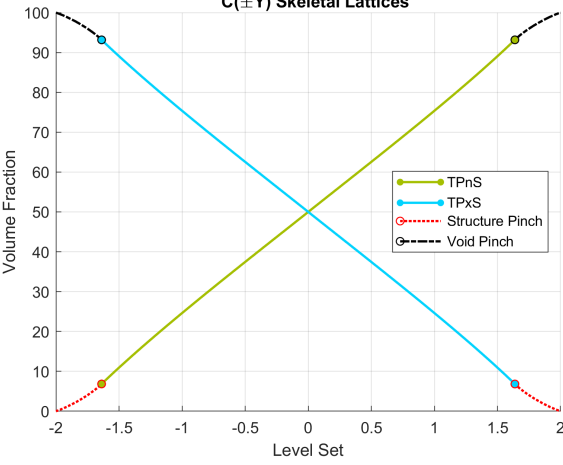
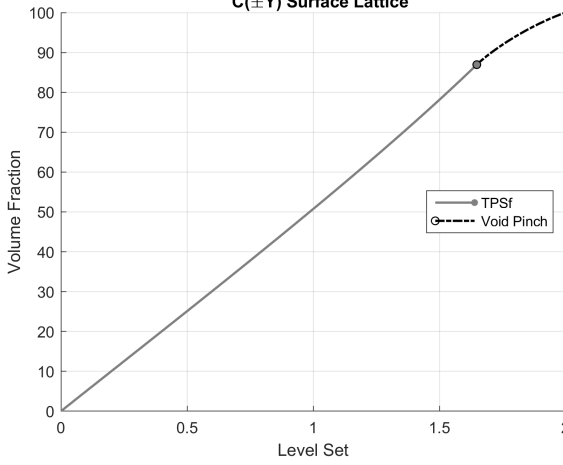
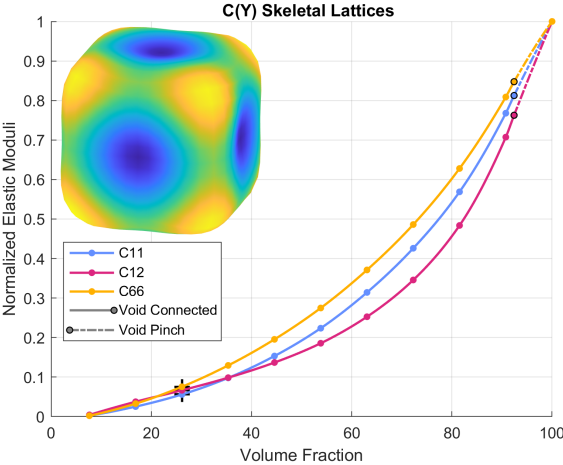
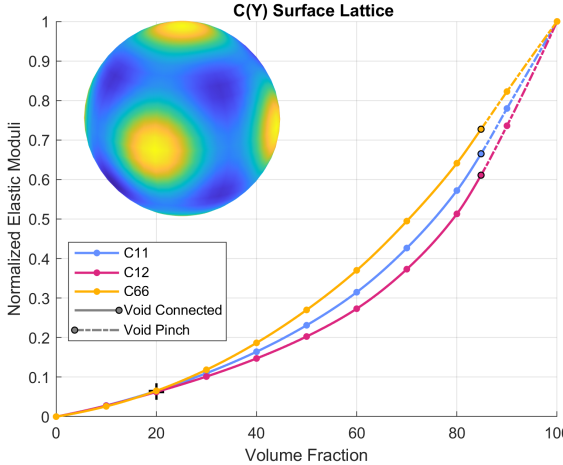
2.21 $\pm Y$

Table 25: Summary for the $\pm Y$ Surface

Alternative Names	
PMY, $(F_{xxx})^*$	
Recommended Equation	
$2(C_x C_y C_z) + (S_{2x} S_y + S_{2y} S_z + S_x S_{2z}) = t$	(36)
TPnS/TPxS	TPSf
Volume Fraction Plots	
Effective Elastic Moduli Plots	
Critical Level Set Values	
$t_{\text{crit}} = \pm 2.828$ $t_{\text{pinch}} = \pm 0.378$ $VF_{\text{skel,pinch}} = 34.38\%$	

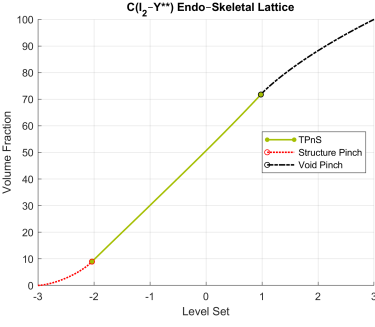
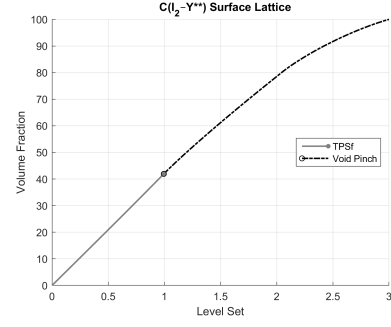
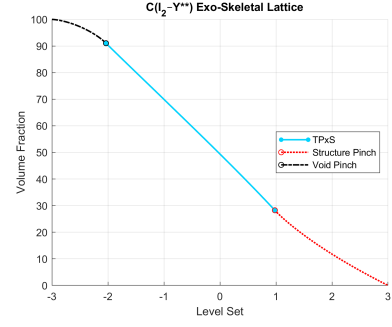
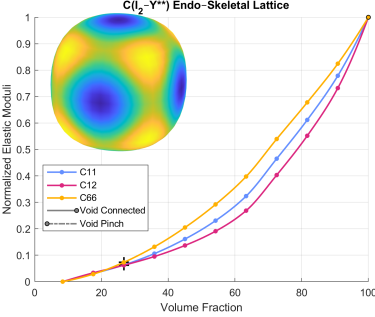
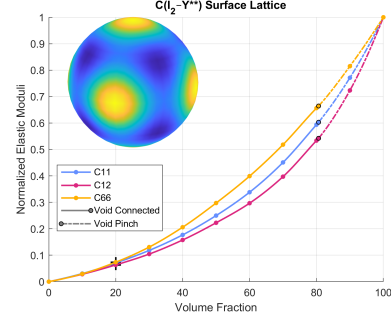
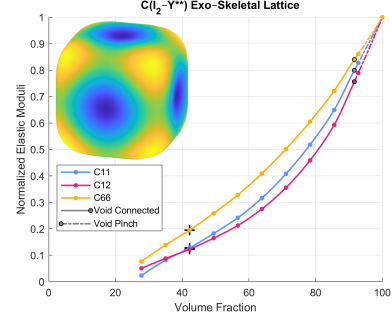
2.22 C($\pm Y$)

Table 26: Summary for the C($\pm Y$) Surface

Alternative Names	
Complementary $\pm Y$, $(FF_{xxx})^*$	Recommended Equation
$-2(C_xC_yC_z) + (S_{2x}S_y + S_{2y}S_z + S_xS_{2z}) = t$	(37)
Volume Fraction Plots	
	
Effective Elastic Moduli Plots	
	
Critical Level Set Values	
$t_{\text{crit}} = \pm 2.000$ $t_{\text{pinch}} = \pm 1.653$ $VF_{\text{skel,pinch}} = 6.342\%$	

2.23 C (I_2 -Y**)

Table 27: Summary for the C (I_2 -Y**) Surface

Alternative Names		
Complementary I_2 -Y**, S*-Y _{xxx}		
Recommended Equation		
$2(S_{2x}C_yS_z + S_xS_{2y}C_z + C_xS_yS_{2z}) + (C_{2x}C_{2y} + C_{2y}C_{2z} + C_{2x}C_{2z}) = t$ (38)		
TPnS	TPSF	TPxS
Volume Fraction Plots		
		
Effective Elastic Moduli Plots		
		
Critical Level Set Values		
$t_{\text{endo}_{\text{crit}}} = -3.000$	$t_{\text{exo}_{\text{crit}}} = 3.000$	
$t_{\text{endo}_{\text{pinch}}} = -2.062$	$t_{\text{exo}_{\text{pinch}}} = 0.999$	
$VF_{\text{endo}_{\text{pinch}}} = 8.384$	$VF_{\text{exo}_{\text{pinch}}} = 27.79$	

The C (I_2 -Y**) and I_2 -Y** surfaces were discussed in von Schnering and Nesper (1991), von Schnering et al. (1991). The name I_2 -Y** is derived from the points used to generate the approximation, and C (I_2 -Y**) is its complement (von Schnering et al., 1991). The I_2 -Y** surface is not given its own subsection, and instead is discussed in Section 2.28 alongside the more common Double Gyroid which is nearly identical to it.

An equation of the same form as Eq. 38, with a coefficient of five on the first term is presented by Hoffman et al. (2003b) as another equation for the G' surface. The geometry generated differs from both Eq. 29 for G' and Eq. 38 for C (I_2 -Y**), and is discussed in Section 2.16 with the new name G'_2.

Between $t_{\text{exo}_{\text{pinch}}}$ and $t_{\text{exo}_{\text{crit}}}$, the TPxS of the C (I_2 -Y**) becomes a series of irregular non-intersecting beams. This is shown in Fig. 7, where six non-connecting beams span the unit cell, connecting to adjacent cells but not to one another. We note this behavior because as a consequence, the TPnS will not have closed void volumes even at level sets above $t_{\text{exo}_{\text{pinch}}}$, and the TPSF produces no closed void volumes until $t \geq |t_{\text{endo}_{\text{pinch}}}|$, even though $|t_{\text{endo}_{\text{pinch}}}| > |t_{\text{exo}_{\text{pinch}}}|$. This is reflected in the transition from “Void Connected” to “Void Pinch” in the Effective Elastic Moduli Plots in Table 26. A second pinch value is not listed in Table 27 for C (I_2 -Y**), even though the TPxS remains connected until $t_{\text{exo}_{\text{crit}}}$, because of the poor

connectivity and if struts of this configuration are needed, it would likely be better to model them with a uniform shape and profile.

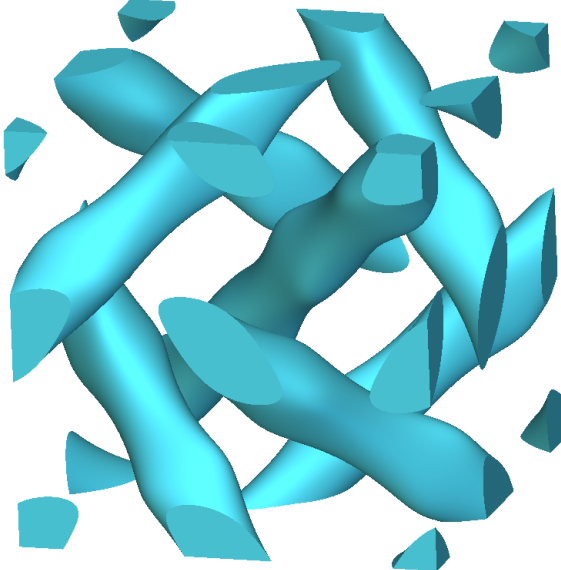


Figure 7: The TPxS of the modeled at $t = 1.5$, which falls between $t_{\text{exo}_{\text{pinch}}}$ and $t_{\text{exo}_{\text{crit}}}$. In this range, the lattice does not lose all connectivity, however, it becomes a series of angled non-intersecting struts with irregular size and shape.

Remainder of page intentionally left blank

2.24 W

Table 28: Summary for the W Surface

Alternative Names	
W^*	
Recommended Equation	
$(C_{2x}C_y + C_{2y}C_z + C_xC_{2z}) - (C_xC_{2y} + C_yC_{2z} + C_{2x}C_z) = t$	(39)
TPnS/TPxS	TPSf
Volume Fraction Plots	
Effective Elastic Moduli Plots	
Critical Level Set Values	
$t_{\text{crit}} = \pm 4.000$ $t_{\text{pinch}} = \pm 0.000$ $VF_{\text{skel,pinch}} = 50.00\%$	

The W-surface is congruent and the TPnS and TPxS are connected only for $VF > 0.5$. As a result, regardless of which of the three lattices are generated, there will always be closed internal regions. The number of regions will be double for the TPSf because it will have regions associated with both the TPnS and TPxS. As a result, W Lattices would likely not be suitable for current AM processes where feed material would be trapped (e.g. Powder Bed Fusion, or Vat Photopolymerization) without modification, or where overhangs are not possible (e.g. Material Jetting).

2.25 Q^*

Table 29: Summary for the Q^* Surface

Alternative Names	
ST1 Recommended Equation	
$(C_x - 2C_y)C_z - \sqrt{3}S_z(C_{x-y} - C_x) + C_{x-y}C_z = t$	(40)
TPnS/TPxS	TPSf
Volume Fraction Plots	
<p>Q* Skeletal Lattices</p> <p>Volume Fraction</p> <p>Level Set</p>	<p>Q* Surface Lattice</p> <p>Volume Fraction</p> <p>Level Set</p>
Effective Elastic Moduli Plots	
<p>Q* Skeletal Lattices</p> <p>Normalized Elastic Moduli</p> <p>Volume Fraction</p> <p>C11, C12, C66, Void Connected, Void Pinch</p>	<p>Q* Surface Lattice</p> <p>Normalized Elastic Moduli</p> <p>Volume Fraction</p> <p>C11, C12, C66, Void Connected, Void Pinch</p>
Critical Level Set Values	
$t_{\text{crit}} = \pm 4.000$ $t_{\text{pinch}} = \pm 2.249$ $VF_{\text{skel,pinch}} = 10.79\%$	

We note that the anisotropy surfaces shown in Table 29 are very unique, and recommend further investigation of the anisotropy of these lattices.

2.26 C(G)

Table 30: Summary for the C(G) Surface

Alternative Names	
Complementary G, C(Y**), Complementary Y**	
Recommended Equation	
$3(S_xC_y + S_yC_z + C_xS_z) + 2(S_{3x}C_y + S_{3y}C_z + C_xS_{3z}) - 2(S_xC_{3y} + S_yC_{3z} + C_{3x}S_z) = t \quad (41)$	
TPnS/TPxS	TPSf
Volume Fraction Plots	
<p>C(G) Skeletal Lattices</p> <p>Volume Fraction</p> <p>Level Set</p> <p>Legend: TPnS (green solid line), TPxS (cyan solid line), Structure Pinch (red dotted line), Void Pinch (black dashed line).</p>	<p>C(G) Surface Lattice</p> <p>Volume Fraction</p> <p>Level Set</p> <p>Legend: TPSf (grey solid line with dots), Void Pinch (black dashed line).</p>
Effective Elastic Moduli Plots	
<p>C(G) Skeletal Lattices</p> <p>Normalized Elastic Moduli</p> <p>Volume Fraction</p> <p>Legend: C11 (blue circles), C12 (pink circles), C66 (orange circles), Void Connected (black line with dots), Void Pinch (black dashed line).</p>	<p>C(G) Surface Lattice</p> <p>Normalized Elastic Moduli</p> <p>Volume Fraction</p> <p>Legend: C11 (blue circles), C12 (pink circles), C66 (orange circles), Void Connected (black line with dots), Void Pinch (black dashed line).</p>
Critical Level Set Values	
$t_{\text{crit}} = \pm 10.500$ $t_{\text{pinch}} = \pm 3.419$ $VF_{\text{skel,pinch}} = 15.84\%$	
$t_{\text{pinch2}} = \pm 4.242$ $VF_{\text{skel,pinch2}} = 9.979$	

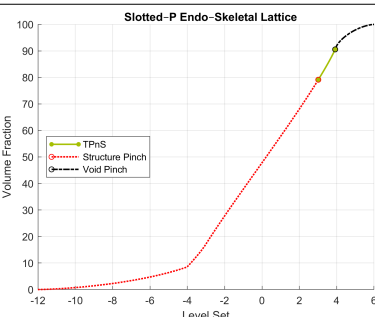
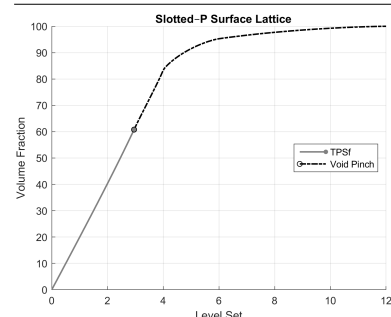
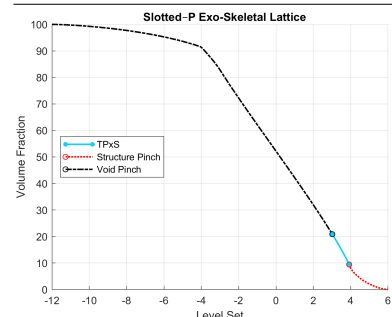
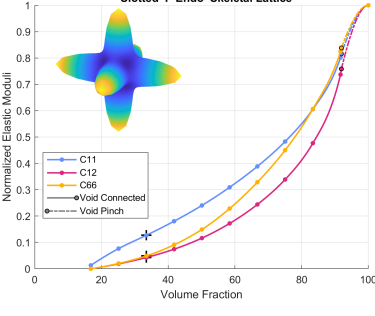
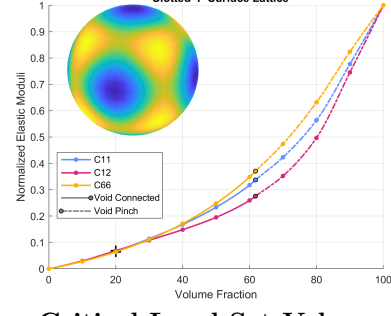
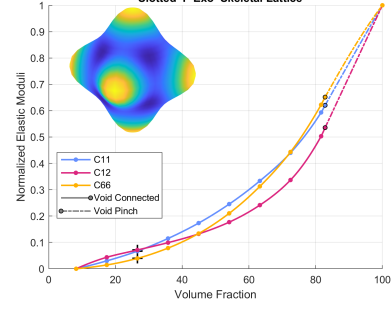
The lattices of C(G) surface generated from Eq. 41 have a unique property (that is also seen in the C(Y), D', and C(D) lattices) where, as the magnitude of the level set increases, the surface pinches off in such a way that there still exists a connected structure that spans the domain but with additional disconnected “floating” volumes also. The disconnected volumes can be removed from the lattice allowing for lattices to be generated from this approximation at a broader range of volume fractions. This is demonstrated in Fig. 2

with the TPxS of the C(Y) surface. It is important to note that the connectivity of the lattice changes significantly when this happens and a large step change in the properties is likely also. For the C(G) surface, it maintains some connectivity until secondary level sets of $t_{\text{exo}_{\text{pinch}2}} = 4.242$ or $t_{\text{endo}_{\text{pinch}2}} = -4.242$, with a volume fraction as low as $VF_{\text{exo}_{\text{pinch}2}} = 9.979$ or $VF_{\text{endo}_{\text{pinch}2}} = 9.979$ with the “floating” material removed. The pinching behavior of this surface differs from the Lidinoid, Split-P, G', and G'_2 surfaces which separate into finite numbers of connected structures (without “floating” volumes) between their respective first and second pinch level sets.

Remainder of page intentionally left blank

2.27 Slotted-P

Table 31: Summary for the Slotted-P Surface

Alternative Names		
$W_zI - W_{xx}$		
Recommended Equation		
	$\begin{aligned} -2(C_xC_y + C_yC_z + C_xC_z) - 2(C_{2x} + C_{2y} + C_{2z}) + \\ (C_{2x}C_y + C_{2y}C_z + C_xC_{2z}) - (C_xC_{2y} + C_yC_{2z} + C_{2x}C_z) = t \end{aligned} \quad (42)$	
TPnS	TPSF	TPxS
Volume Fraction Plots		
		
Effective Elastic Moduli Plots		
		
Critical Level Set Values		
$t_{\text{endo}_{\text{crit}}} = -12.00$	$t_{\text{exo}_{\text{crit}}} = 6.000$	
$t_{\text{endo}_{\text{pinch}}} = -2.999$	$t_{\text{exo}_{\text{pinch}}} = 3.999$	
$VF_{\text{endo}_{\text{pinch}}} = 16.82$	$VF_{\text{exo}_{\text{pinch}}} = 8.209$	

We propose the name “Slotted-P” for this surface and lattices to replace the name $W_zI - W_{xx}$ given by (von Schnering et al., 1991) because the unit cell of the Slotted-P (shown in Table 35) looks similar to eight cells of the P-surface with two pairs of the profiles intersecting each face of the cubic cell being joined. The Slotted-P surface, unlike the P-surface, is not congruent.

2.28 Double Versions of the Gyroid, D, and P

For the Gyroid, D-surface, and P-surface, there have been derived a single equation that produces two independent triply periodic surfaces offset from the zero level set known as the double of the surface. This has a similar effect as applying equal and opposite level sets to the standard equations presented in Sections 2.1 to 2.3. However, due to the difference in the low order Fourier series fit used, there are discrepancies between the structures produced this way. The discrepancies are a function of the level set, which can be seen in Fig. 8 for an extreme case for the P and Double P surfaces. For completeness, these three commonly seen double equations are included here (Table 32). However, we recommend using two “single” lattices with different offsets to achieve more predictable results, which avoids the type of issues shown in Fig. 8, especially with non-uniform lattices.

The equation for the Double Gyroid also appears in von Schnering and Nesper (1991) under the name $I_2\text{-}Y^{**}$, with the first coefficient changed to 2 and the whole equation multiplied by -1 . The surfaces produced by the two different sets of coefficients were not compared as the Double equations are not typically recommended. Equation 17 for approximating the Lidinoid also has the same form as the equation for the Double Gyroid, however the difference between coefficients used results in a significantly different geometry.

Table 32: Double surface equations for the Gyroid, D, and P surfaces

Double Gyroid	$2.75(S_{2x}C_yS_z + S_{2y}C_xS_z + S_{2z}S_yC_x) - (C_{2x}C_{2y} + C_{2y}C_{2z} + C_{2z}C_{2x}) = t$
Double D	$(S_{2x}S_{2y} + S_{2y}S_{2z} + S_{2z}S_{2x}) + C_{2x}C_{2y}C_{2z} = t$
Double P	$0.5(C_xC_y + C_yC_z + C_zC_x) + 0.2(C_{2x} + C_{2y} + C_{2z}) = t$

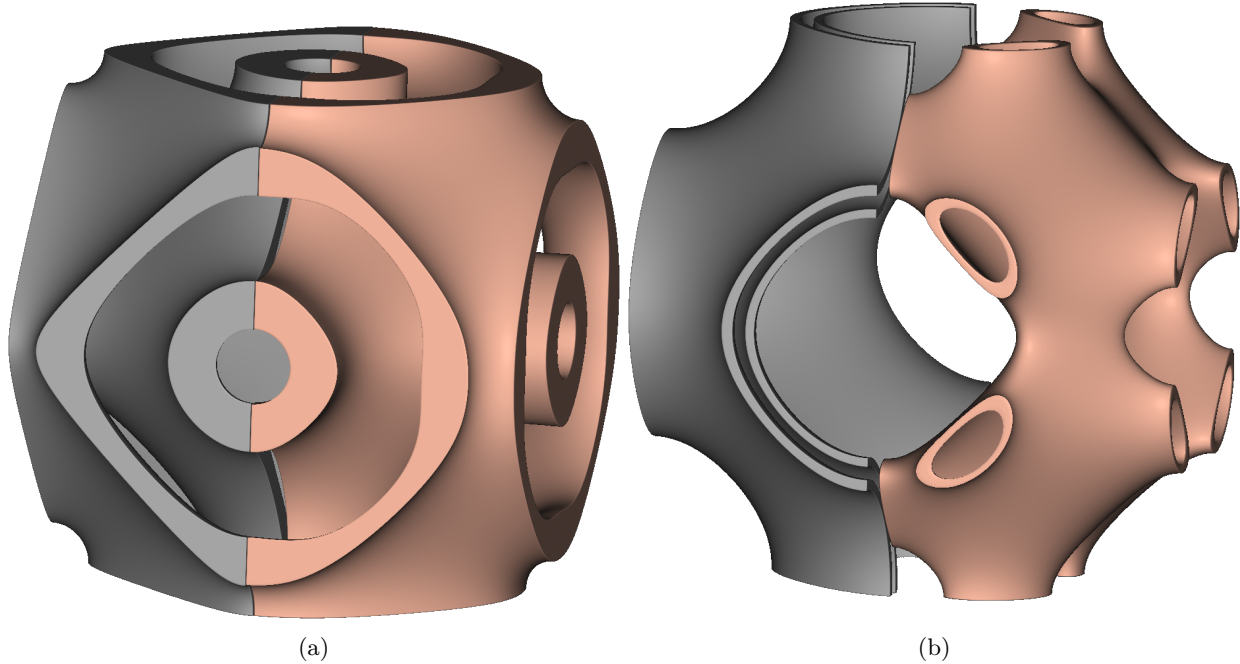


Figure 8: (a) half periods of two TPSf of the P surface at level sets of $[0.5, 9]$ and $[-0.9, -0.5]$ in gray mirroring a half period of the TPSf of the Double P Surface at level sets of $[-0.2, 0.02]$ and (b) again at a level sets of $[-0.2, -0.1]$ and $[0.05, 0.175]$ for the two P surfaces and $[-0.36, -0.34]$ for the Double P Surface. In (a) the two methods of generating lattices produce similar results, whereas in (b) difference in the lattice produced by the two equations is significant with the Double P Surface differing significantly from the intended shape.

2.29 Modifications to Surface Equations at Low Volume Fractions

As noted, for each surface in this appendix, the skeletal lattices pinch off at different volume fractions, which (typically) occurs prior to reaching a volume fraction of zero. In [Section 2.1](#), we include a piecewise modification to the accepted Gyroid equation (derived by [Li et al. \(2018\)](#)) that prevents pinch off of the skeletal lattices, enabling lower volume fractions.

For the Gyroid and D Surfaces, [Fisher et al. \(2022\)](#) determined the mean curvature of the approximations in [Eqs. 8](#) and [12](#) analytically. The mean curvature equations were then used to define new variants of the lattices referred to as the MC Gyroid and MC D-surface that shares the same topology, and have similar geometry. however, The MC variants are able to achieve lower volume fractions prior to pinch-off compared to the standard variants. The properties of these new lattices were not yet studied.

[Michielsen and Kole \(2003\)](#) talks about “tubular” versions of the Gyroid, D-surface, and P-surface lattices. They cite [Hoffman et al. \(2000\)](#) as their source where they are referred to as “Skeletal Graphs Approximated by Level Surfaces”. Note that even though the three original surfaces are congruent, this is not true for the tubular/skeletal graph versions which produce distinct TPnS and TPxS, with the TPxS displaying the desired tubular/skeletal graph geometry. [Hoffman et al. \(2000\)](#) includes also an equation for a similar modification to the IWP which is intentionally omitted here because it is [Eq. 14](#) multiplied by a factor of five. We do note that [Eq. 14](#) is already able to achieve exceedingly small volume fractions when modeling the TPxS (see [Fig. 1](#)).

Table 33: “Tubular”/“Skeletal Graph” versions of surface equations for generating skeletal lattices of the Gyroid, D, and P surfaces ([Hoffman et al., 2000](#), [Michielsen and Kole, 2003](#)).

Tubular Gyroid	$10(C_x S_y + C_y S_z + C_z S_x) - 0.5(C_{2x} C_{2y} + C_{2y} C_{2z} + C_{2z} C_{2x}) - 14$
Tubular D	$10(S_X S_Y S_Z + S_X C_Y C_Z + C_X S_Y C_Z + C_X C_Y S_Z) - 0.7(C_{4x} + C_{4y} + C_{4z}) - 11$
Tubular P	$10(C_x + C_y + C_z) - 5.1(C_x C_y + C_y C_z + C_z C_x) - 14.6$

In the Tubular D equation, $X = x - \pi/4$, $Y = y - \pi/4$, and $Z = z - \pi/4$

Remainder of page intentionally left blank

3 Images of Lattice Structures and Related TPMS

The lattice structures shown in this document are produced in the nTopology software using custom TPMS lattice generation blocks that are included in this dataset. Representations of the TPMS surfaces in the first column are produced using Ken Brakke's Surface Evolver tool ([Brakke, c](#)). When available evolver files for each TPMS were sourced from Ken Brakke's website ([Brakke, a](#)) and modifications were made to match the unit cell, colors, and rotation of the surface to the lattice images in the remaining columns before evolving the surface till there was no discernible tessellation on the surface at the viewing resolution.

We note again, as defined in [Section 1](#), that the TPnS and TPxS of each surface are defined mathematically and not visually. For some surfaces with the selected unit cell, the naming convention can appear counterintuitive.

With two exceptions, the images in [Table 35](#) were generated using a cubic unit cell that is aligned with the Cartesian coordinate system that has limits of $\pm P/2$ in x , y and z . Where P is the periodicity of the surface and lattices which is equal in x , y , and z . The OCTO surface is produced using a cubic unit cell with limits of 0 and P in x , y , and z to match existing imagery in the literature. The C(D) surface, in addition to the standard cubic unit cell, is shown in a unit cell made of a rhombic dodecahedron (which like a cube is a space-filling polyhedron). This is included to highlight geometric differences between the TPMS and the lattices generated using the approximation in [Eq. 27](#).

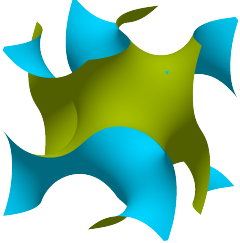
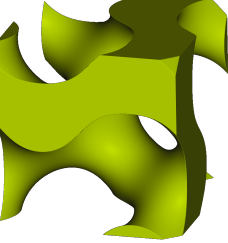
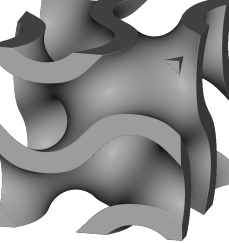
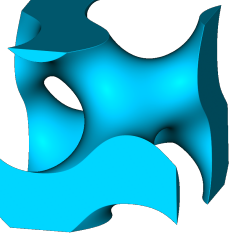
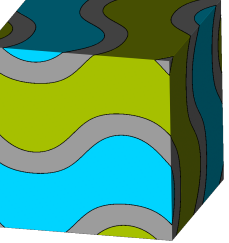
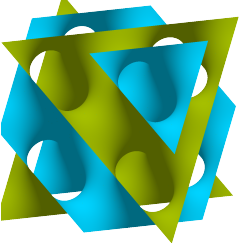
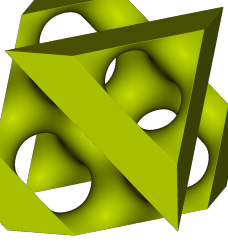
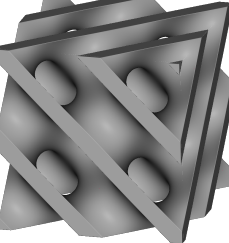
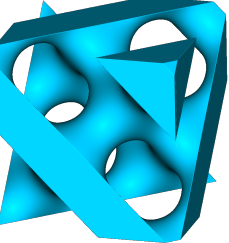
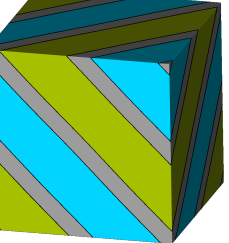
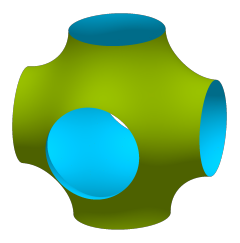
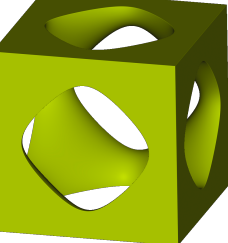
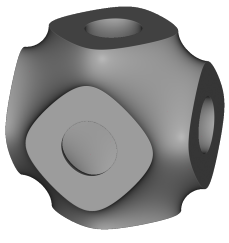
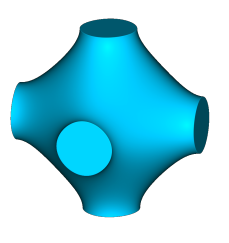
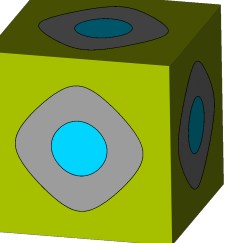
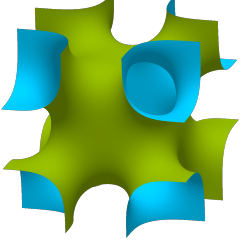
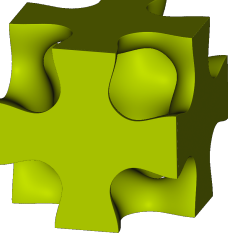
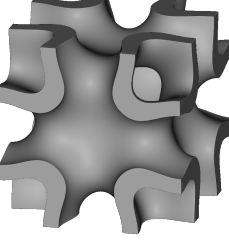
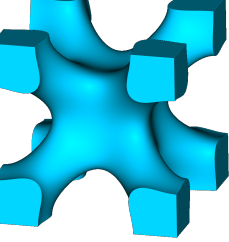
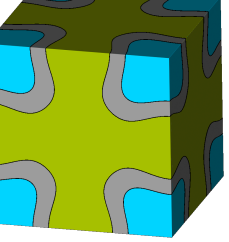
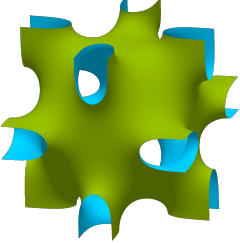
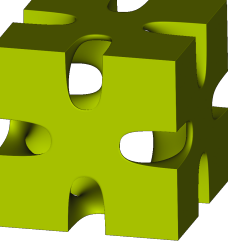
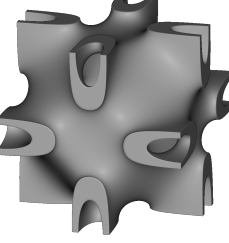
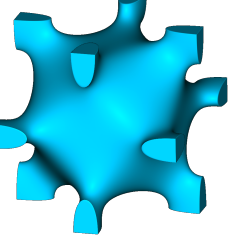
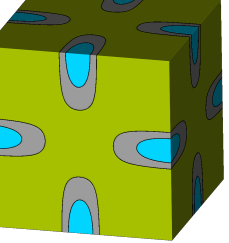
The three types of lattices in this dataset are each given a unique color to aid in differentiation. We recommend keeping this color scheme in future publications for clarity and consistency. The color palette used for the images in this dataset was selected to be colorblind-friendly and visually appealing. They are not perfect, as we were selecting from those available in the nTopology software tool. The images were enhanced by maximizing the chroma range while keeping the hue and luminosity constant. The resulting colors are given in [Table 34](#) for future use.

Table 34: Colors used for the visualization of TPMS and lattices.

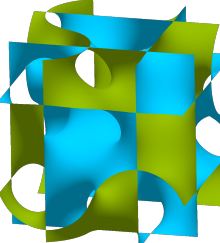
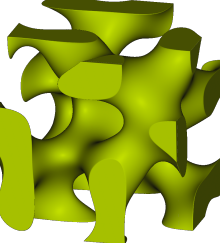
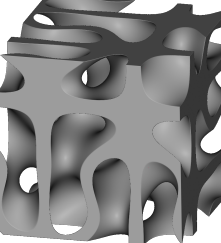
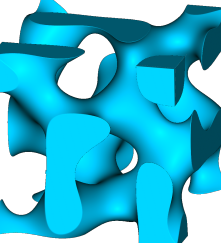
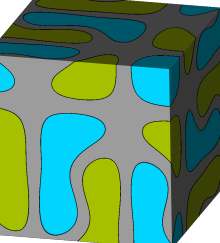
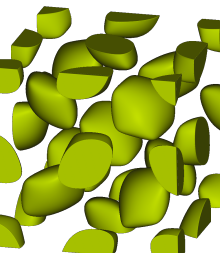
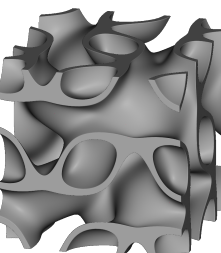
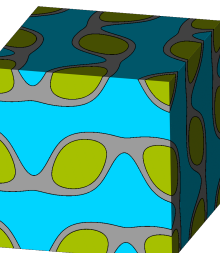
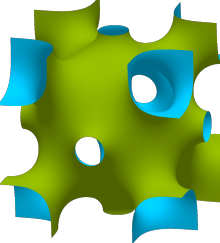
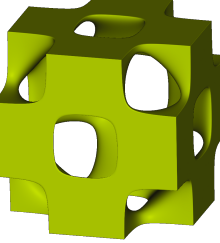
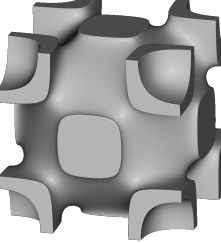
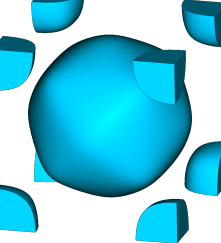
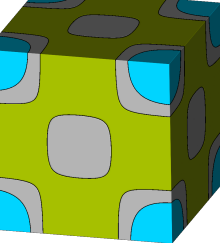
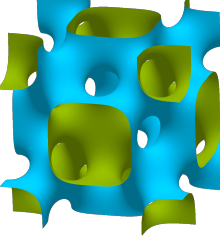
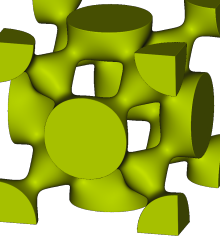
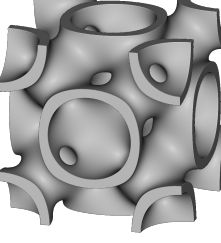
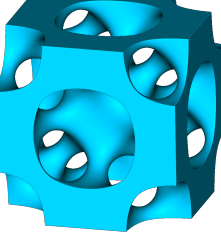
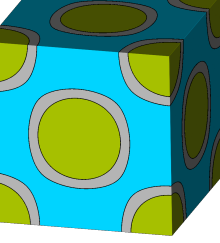
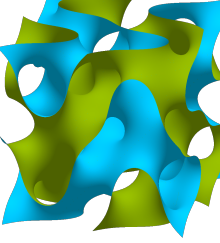
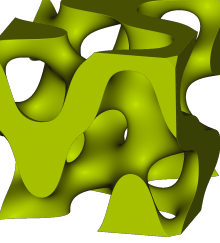
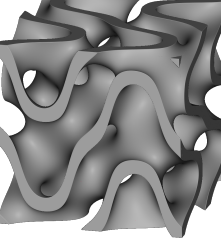
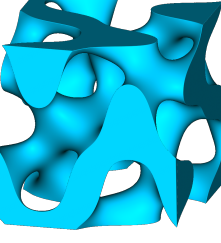
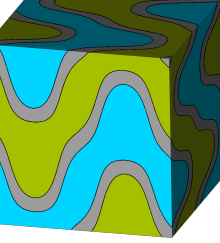
Lattice	Hue	RGB Values	Hexadecimal Code
TPnS	Green	(165, 191, 1)	#A5BF01
TPsf	Gray	(128, 128, 128)	#808080
TPxS	Blue	(1, 211, 254)	#01D3FE

Remainder of page intentionally left blank

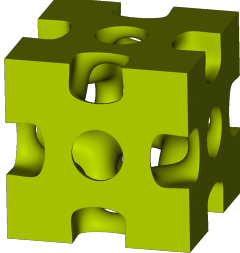
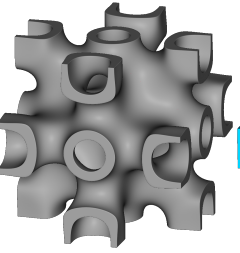
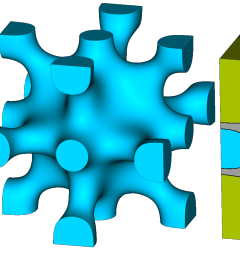
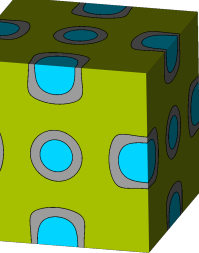
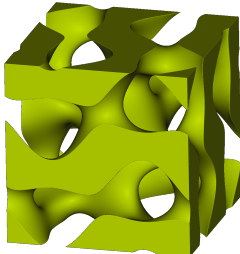
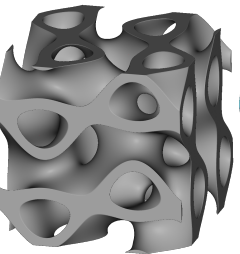
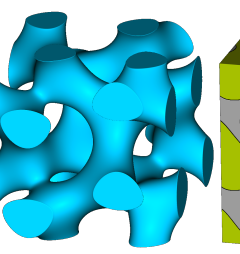
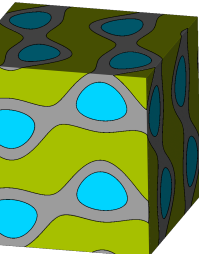
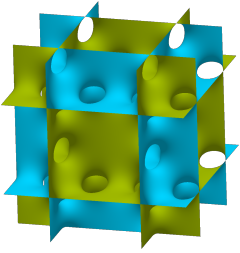
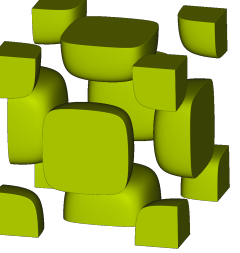
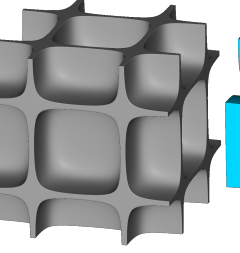
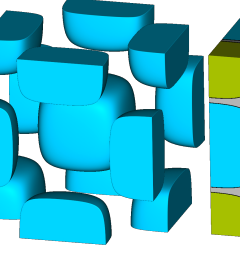
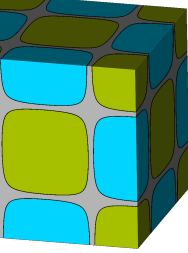
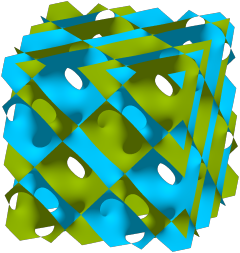
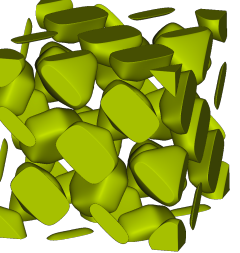
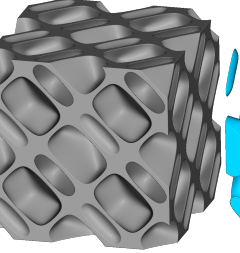
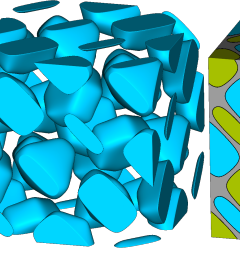
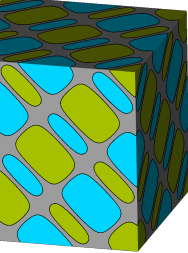
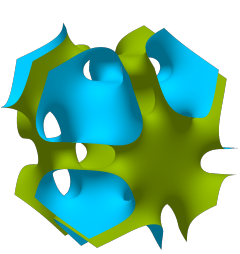
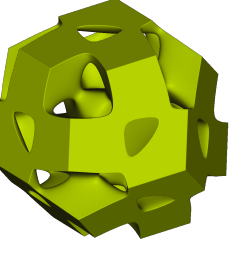
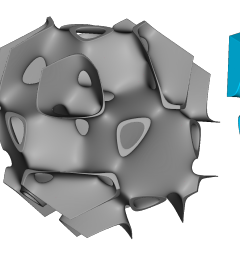
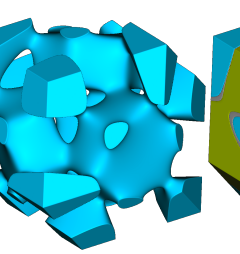
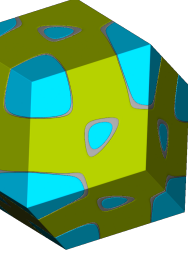
Table 35: Images of TPMS & lattices discussed

TPMS	Endo-skeleton (TPnS)	Surface (TPSf)	Exo-skeleton (TPxS)	Combined
		Gyroid		
				
		D-surface		
				
		P-surface		
				
		IWP		
				
		Neovius		
				

Continued

TPMS	Endo-skeleton (TPNs)	Surface (TPSf)	Exo-skeleton (TPxS)	Combined
		C(Y)-Surface		
				
No Image		Lidinoid		
		OCTO		
				
		FRD		
				
		S-Surface		
				

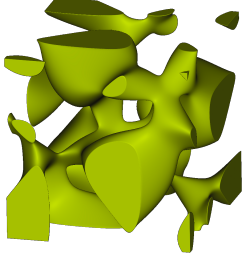
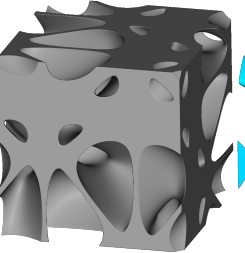
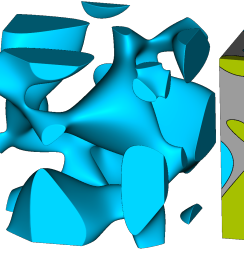
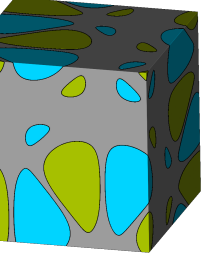
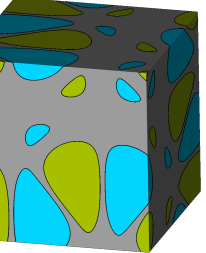
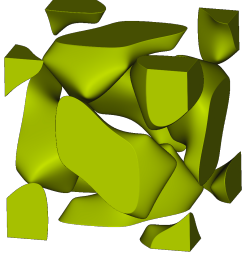
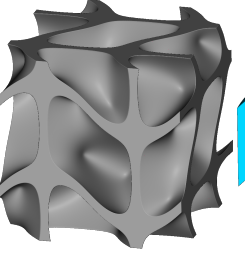
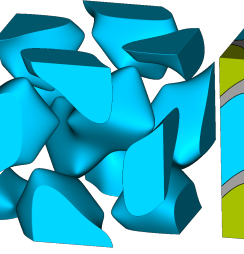
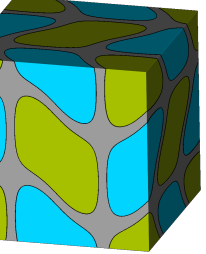
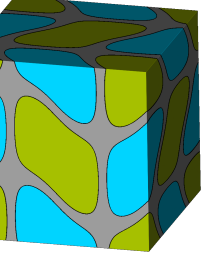
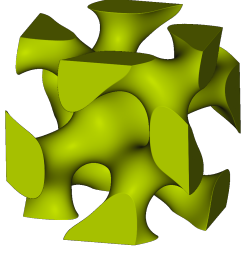
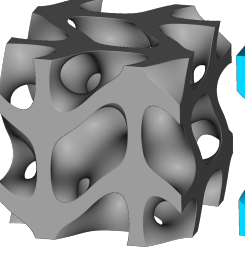
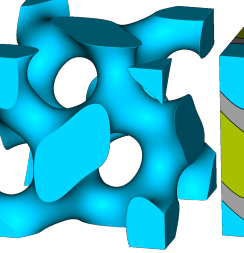
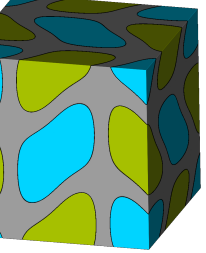
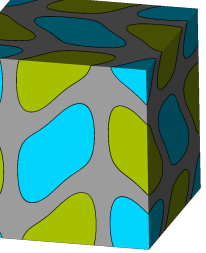
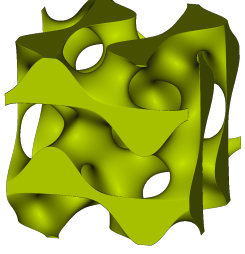
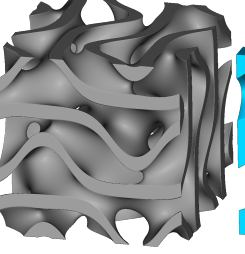
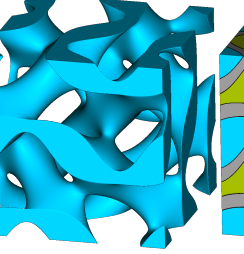
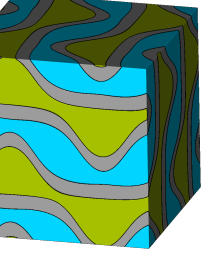
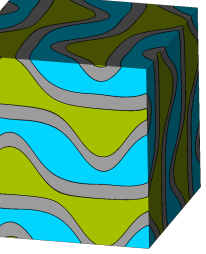
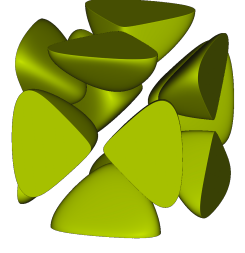
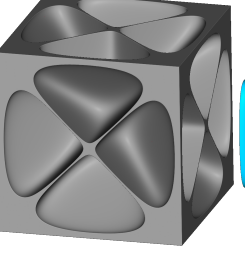
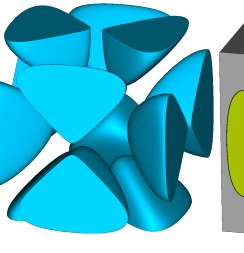
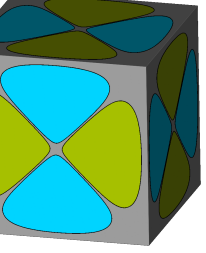
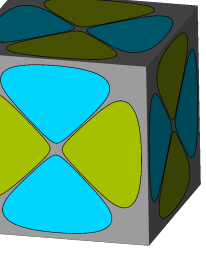
Continued

	TPMS	Endo-skeleton (TPnS)	Surface (TPSf)	Exo-skeleton (TPxS)	Combined
No Image			P+C(P)		
					
No Image			Split-P		
					
			F-Surface		
					
			C(D)-Surface Cubic Unit Cell		
					
			Rhombic Dodecahedral Unit Cell		
					

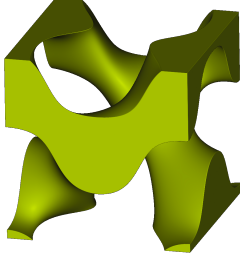
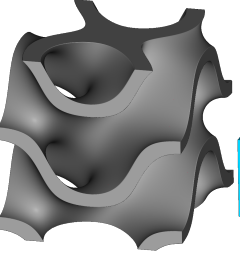
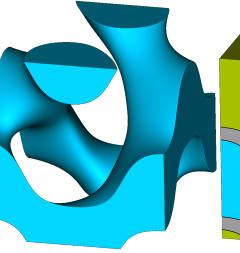
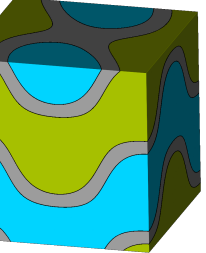
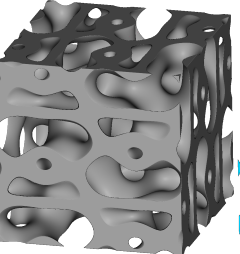
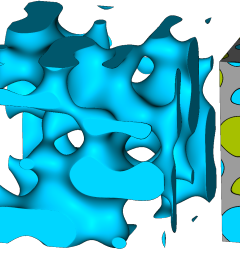
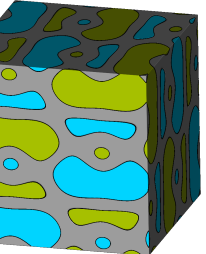
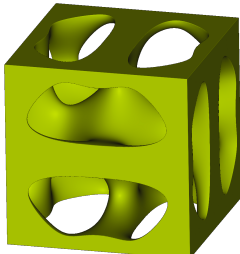
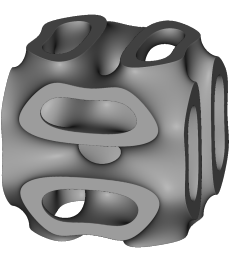
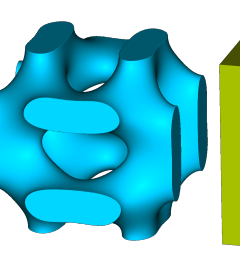
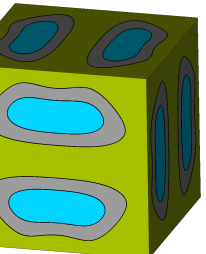
Continued

	TPMS	Endo-skeleton (TPnS)	Surface (TPSf)	Exo-skeleton (TPxS)	Combined
No Image			G'-Surface		
No Image			G'_2-Surface		
No Image			D'-Surface		
No Image			K-Surface		
No Image			C(S)-Surface		

Continued

	TPMS	Endo-skeleton (TPNs)	Surface (TPSf)	Exo-skeleton (TPxS)	Combined
No Image					
No Image					
No Image					
No Image					
No Image					

Continued

TPMS	Endo-skeleton (TPnS)	Surface (TPSf)	Exo-skeleton (TPxS)	Combined
No Image				
No Image				
No Image				

Remainder of page intentionally left blank

Bibliography

- J. Austermann, A. J. Redmann, V. Dahmen, A. L. Quintanilla, S. J. Mecham, and T. A. Osswald. Fiber-reinforced composite sandwich structures by co-curing with additive manufactured epoxy lattices. *Journal of Composites Science*, 3(2):53, 2019. doi:[10.3390/jcs3020053](https://doi.org/10.3390/jcs3020053).
- K. A. Brakke. Triply Periodic Minimal Surfaces, a. URL <https://facstaff.susqu.edu/brakke/evolver/examples/periodic/periodic.html>.
- K. A. Brakke. Triplane Triply Periodic Minimal Surfaces, b. URL <http://facstaff.susqu.edu/brakke/evolver/examples/periodic/periodic.html#triplane>.
- K. A. Brakke. The surface evolver. *Experimental mathematics*, 1(2):141–165, 1992c. doi:[10.1080/10586458.1992.10504253](https://doi.org/10.1080/10586458.1992.10504253).
- X. Chen, M. Hu, Y. Sun, J. Yang, L. Bai, and Y. Xiong. Wide-range tuning of the mechanical properties of tpms lattice structures through frequency variation. *Materials & Design*, 224:111370, 2022. doi:[10.1016/j.matdes.2022.111370](https://doi.org/10.1016/j.matdes.2022.111370).
- K. Dutkowski, M. Kruzel, and K. Rokosz. Review of the state-of-the-art uses of minimal surfaces in heat transfer. *Energies*, 15(21):7994, 2022. doi:[10.3390/en15217994](https://doi.org/10.3390/en15217994).
- J. W. Fisher, S. W. Miller, J. Bartolai, and M. A. Yukish. Using Mean Curvature of Implicitly Defined Minimal Surface Approximations to Generate New Unit Cells for Lattice Design. In *Proceedings of the 33rd Annual International Solid Freeform Fabrication Symposium*, pages 2233–2243, 07 2022. doi:[10.26153/tsw/44431](https://doi.org/10.26153/tsw/44431).
- R. Goldman. Curvature formulas for implicit curves and surfaces. *Computer Aided Geometric Design*, 22(7):632–658, 2005. doi:[10.1016/j.cagd.2005.06.005](https://doi.org/10.1016/j.cagd.2005.06.005).
- X. Guo, X. Zheng, Y. Yang, X. Yang, and Y. Yi. Mechanical behavior of tpms-based scaffolds: A comparison between minimal surfaces and their lattice structures. *SN Applied Sciences*, 1(10):1145, 2019. doi:[10.1007/s42452-019-1167-z](https://doi.org/10.1007/s42452-019-1167-z).
- D. A. Hoffman, J. T. Hoffman, M. Weber, M. Trazet, M. Wohlgemuth, E. Boix, M. Callahan, E. Thayer, and F. Wei. Skeletal Graphs Approximated by Level Surfaces. *The Scientific Graphics Project*. Mathematical Sciences Research Institute, 2000. URL <https://www.msri.org/publications/sgp/jim/geom/level/skeletal/mainc.html>.
- D. A. Hoffman, J. T. Hoffman, M. Weber, M. Trazet, M. Wohlgemuth, E. Boix, M. Callahan, E. Thayer, and F. Wei. The Split P Surface. *The Scientific Graphics Project*. Mathematical Sciences Research Institute, 2003a. URL <https://www.msri.org/publications/sgp/jim/papers/morphbysymmetry/splitp/index.html>.
- D. A. Hoffman, J. T. Hoffman, M. Weber, M. Trazet, M. Wohlgemuth, E. Boix, M. Callahan, E. Thayer, and F. Wei. Table of Surfaces. *The Scientific Graphics Project*. Mathematical Sciences Research Institute, 2003b. URL <https://www.msri.org/publications/sgp/jim/papers/morphbysymmetry/table/index.html>.
- M.-T. Hsieh and L. Valdevit. Minisurf—A minimal surface generator for finite element modeling and additive manufacturing. *Software Impacts*, 6:100026, 2020. doi:[10.1016/j.simpa.2020.100026](https://doi.org/10.1016/j.simpa.2020.100026).
- H. Karcher. The triply periodic minimal surfaces of Alan Schoen and their constant mean curvature companions. *Manuscripta mathematica*, 64(3):291–357, 1989. doi:[10.1007/BF01165824](https://doi.org/10.1007/BF01165824).
- P. Karlsson, L. Pejryd, and N. Strömberg. Generative design optimization and characterization of triple periodic lattice structures in alsi10mg. In *Industrializing Additive Manufacturing: Proceedings of AMPA2020*, pages 3–16. Springer, 2021. doi:[10.1007/978-3-030-54334-1_1](https://doi.org/10.1007/978-3-030-54334-1_1).

- E. Koch and W. Fischer. On 3-periodic minimal surfaces with non-cubic symmetry. *Zeitschrift für Kristallographie-Crystalline Materials*, 183(1-4):129–152, 1988. doi:[10.1524/zkri.1988.183.14.129](https://doi.org/10.1524/zkri.1988.183.14.129).
- E. Koch and W. Fischer. Triply periodic minimal balance surfaces: a correction. *Acta Crystallographica Section A: Foundations of Crystallography*, 49(1):209–210, 1993. doi:[10.1107/S0108767392007591](https://doi.org/10.1107/S0108767392007591).
- D. Li, W. Liao, N. Dai, G. Dong, Y. Tang, and Y. M. Xie. Optimal design and modeling of gyroid-based functionally graded cellular structures for additive manufacturing. *Computer-Aided Design*, 104:87–99, 2018. doi:[10.1016/j.cad.2018.06.003](https://doi.org/10.1016/j.cad.2018.06.003).
- S. Lidin and S. Larsson. Bonnet transformation of infinite periodic minimal surfaces with hexagonal symmetry. *Journal of the Chemical Society, Faraday Transactions*, 86(5):769–775, 1990. doi:[10.1039/FT9908600769](https://doi.org/10.1039/FT9908600769).
- F. Liu, D. Z. Zhang, P. Zhang, M. Zhao, and S. Jafar. Mechanical properties of optimized diamond lattice structure for bone scaffolds fabricated via selective laser melting. *Materials*, 11(3):374, 2018. doi:[10.3390/ma11030374](https://doi.org/10.3390/ma11030374).
- F. Liu, T. Zhou, T. Zhang, H. Xie, Y. Tang, and P. Zhang. Shell offset enhances mechanical and energy absorption properties of slm-made lattices with controllable separated voids. *Materials & Design*, 217: 110630, 2022. doi:[10.1016/j.matdes.2022.110630](https://doi.org/10.1016/j.matdes.2022.110630).
- E. A. Lord and A. L. Mackay. Periodic minimal surfaces of cubic symmetry. *Current Science*, pages 346–362, 2003. URL <https://www.jstor.org/stable/24108665>.
- D. Mahmoud, S. R. S. Tandel, M. Yakout, M. Elbestawi, F. Mattiello, S. Paradiso, C. Ching, M. Zaher, and M. Abdelnabi. Enhancement of heat exchanger performance using additive manufacturing of gyroid lattice structures. *The International Journal of Advanced Manufacturing Technology*, Apr 2023. ISSN 1433-3015. doi:[10.1007/s00170-023-11362-9](https://doi.org/10.1007/s00170-023-11362-9).
- K. Michelsen and J. Kole. Photonic band gaps in materials with triply periodic surfaces and related tubular structures. *Physical Review B*, 68(11):115107, 2003. doi:[10.1103/PhysRevB.68.115107](https://doi.org/10.1103/PhysRevB.68.115107).
- H. Peng, F. Gao, and W. Hu. Design, modeling and characterization on triply periodic minimal surface heat exchangers with additive manufacturing. In *2019 International Solid Freeform Fabrication Symposium*. University of Texas at Austin, 2019. doi:[10.26153/tsw/17483](https://doi.org/10.26153/tsw/17483).
- N. Strömberg. Optimal grading of tpms-based lattice structures with transversely isotropic elastic bulk properties. *Engineering Optimization*, 53(11):1871–1883, 2021. doi:[10.1080/0305215X.2020.1837790](https://doi.org/10.1080/0305215X.2020.1837790).
- H. G. von Schnering and R. Nesper. Nodal surfaces of Fourier series: fundamental invariants of structured matter. *Zeitschrift für Physik B Condensed Matter*, 83(3):407–412, 1991. doi:[10.1007/BF01313411](https://doi.org/10.1007/BF01313411).
- H. G. von Schnering, M. Oehme, and G. Rudolf. Three-dimensional periodic nodal surfaces which envelope the threefold and fourfold cubic rod packings. *Acta chemica scandinavica (Copenhagen. 1989)*, 45(8): 873–876, 1991. doi:[10.3891/acta.chem.scand.45-0873](https://doi.org/10.3891/acta.chem.scand.45-0873).
- M. Wohlgemuth, N. Yuja, J. Hoffman, and E. L. Thomas. Triply periodic bicontinuous cubic microdomain morphologies by symmetries. *Macromolecules*, 34(17):6083–6089, 2001. doi:[10.1021/ma0019499](https://doi.org/10.1021/ma0019499).
- K. Yeranee and Y. Rao. A review of recent investigations on flow and heat transfer enhancement in cooling channels embedded with triply periodic minimal surfaces (tpms). *Energies*, 15(23):8994, 2022. doi:[10.3390/en15238994](https://doi.org/10.3390/en15238994).
- E. Zeleny. Triply Periodic Minimal Surfaces, 2013. URL <https://demonstrations.wolfram.com/TriplyPeriodicMinimalSurfaces/>.